

Deletion of FNDC5/Irisin modifies murine osteocyte function in a sex-specific manner

Anika Shimonty¹, Fabrizio Pin², Matt Prideaux², Gang Peng³, Joshua R Huot², Hyeonwoo Kim⁴, Clifford J Rosen⁵, Bruce M Spiegelman⁶, Lynda F Bonewald^{7*}

¹Indiana Center for Musculoskeletal Health, School of Medicine, Indiana University, IN, 46202, Indianapolis.

²Indiana Center for Musculoskeletal Health, Department of Anatomy, School of Medicine, Indiana University, IN, 46202, Indianapolis.

³Indiana Center for Musculoskeletal Health, Department of Medicine and Molecular Genetics, School of Medicine, Indiana University, IN, 46202, Indianapolis.

⁴Department of Biological Sciences, Korea Advanced Institute of Science and Technology, Daejeon, South Korea.

⁵Maine Medical Center Research Institute, ME, 04074, Scarborough, USA.

⁶Department of Cancer Biology, Dana Farber Cancer Institute and Department of Cell Biology, Harvard University Medical School, MA, 02115, Boston, USA.

⁷Department of Anatomy, Cell Biology and Physiology, Orthopaedic Surgery, School of Medicine, Indiana Center for Musculoskeletal Health, Indiana Center for Musculoskeletal Health, Indiana University, IN, 46202, Indianapolis.

***For correspondence:**

lbnewald@iu.edu (LB)

Abstract

Irisin, released from exercised muscle, has been shown to have beneficial effects on numerous tissues but its effects on bone are unclear. We found significant sex and genotype differences in bone from wildtype (WT) mice compared to mice lacking *Fndc5* (KO), with and without calcium deficiency. Despite their bone being indistinguishable from WT females, KO female mice were partially protected from osteocytic osteolysis and osteoclastic bone resorption when allowed to lactate or when placed on a low-calcium diet. Male KO mice have more but weaker bone compared to WT males, and when challenged with a low-calcium diet lost more bone than WT males. To begin to understand responsible molecular mechanisms, osteocyte transcriptomics was performed. Osteocytes from WT females had greater expression of genes associated with osteocytic osteolysis and osteoclastic bone resorption compared to WT males which had greater expression of genes associated with steroid and fatty acid metabolism. Few differences were observed between female KO and WT osteocytes, but with a low calcium diet, the KO females had lower expression of genes responsible for osteocytic osteolysis and osteoclastic resorption than the WT females. Male KO osteocytes had lower expression of genes associated with steroid and fatty acid metabolism, but higher expression of genes associated with bone resorption compared to male WT. In conclusion, irisin plays a critical role in the development of the male but not the female skeleton and protects male but not female bone from calcium deficiency. We propose irisin ensures the survival of offspring by targeting the osteocyte to provide calcium in lactating females, a novel function for this myokine.

In-text word count (Introduction, Results, and Discussion): 10270

Number of data elements: 1 table, 7 figures.

1 Introduction

2 It is widely accepted that bone and muscle interact mechanically as movement
3 of the skeleton by muscle is essential for life. Less well-known but becoming more
4 generally accepted is that muscle and bone can communicate through secreted factors
5 *Brotto and Bonewald (2015)*; *Bonewald (2019)*. Muscle produces factors such as β -
6 aminoisobutyric Acid (BAIBA) and irisin with exercise, that have positive effects on
7 bone, adipose tissue, brain, and other organs, whereas sedentary muscle produces
8 factors such as myostatin that has negative effects on both bone and muscle *Brotto*
9 *and Bonewald (2015)*; *Karsenty and Mera (2018)*; *Kitase et al. (2018)*; *Bostrom et*
10 *al. (2012)*; *Hamrick et al. (2006)*.

11 Many of the factors secreted by bone are produced by osteocytes, the most
12 abundant and the longest-living bone cell *Bonewald (2011)*; *Dallas et al. (2013)*.
13 These cells are derived from terminally differentiated osteoblasts that become
14 surrounded by the newly mineralizing bone matrix *Dallas et al. (2013)*. Osteocytes
15 are multifunctional and appear to be the major mechanosensory cell in bone
16 *Bonewald (2011)*; *Temiyasathit and Jacobs (2010)*; *Uda et al. (2017)*. Under
17 unloaded conditions, these cells produce sclerostin, a negative regulator of bone
18 formation and Receptor Activator of Nuclear factor Kappa β ligand (RANKL), the
19 major factor that recruits and activates osteoclasts to resorb bone *Nakashima et al.*
20 *(2011)*; *Xiong and O'Brien (2012)*; *Xiong et al. (2015)*; *Ono et al. (2020)*. In
21 contrast, with anabolic mechanical loading, these cells produce factors such as
22 prostaglandin E₂ (PGE₂) that have positive effects on myogenesis and muscle
23 function *Mo et al. (2015)*. Osteocytes play a major role in mineral metabolism,
24 through regulation of both calcium and phosphate homeostasis. Osteocytes secrete
25 Fibroblast Growth Factor 23 to target the kidney to regulate phosphate excretion.
26 Both Parathyroid Hormone (PTH) and Parathyroid related peptide (PTHrP) regulate
27 calcium homeostasis via the PTH type 1 receptor on osteocytes *Feng et al. (2009)*;
28 *Teti and Zallone (2009)*. Under the physiological calcium-demanding condition of
29 lactation, osteocytes respond to PTHrP by removing their surrounding perilacunar
30 matrix to provide calcium for offspring, and upon weaning this perilacunar matrix is
31 rapidly replaced, a process referred to as perilacunar remodeling *Qing and*
32 *Bonewald (2009)*; *Qing et al. (2012)*; *Wysolmerski (2013)*. However, under
33 pathological conditions such as ovariectomy, hyperparathyroidism,
34 hypophosphatemic rickets, and cancer, excessive removal of their perilacunar
35 matrix occurs through osteocytic osteolysis *Tsourdi et al. (2018)*; *Jähn-Rickert and*
36 *Zimmermann (2021)*; *Pin et al. (2021)*; *Shimonty et al. (2023)*. Bone is the largest

37 calcium reservoir in the body and human mothers can lose an average of 250
38 mg/day of calcium in milk, emphasizing the need for a calcium-replete diet to
39 prevent bone loss *Qing et al. (2012)*; *Wysolmerski (2002)*; *Kalkwarf (2004)*. During
40 lactation, PTHrP targets the osteocyte to elevate genes coding for factors necessary
41 for the removal of their calcium-laden periacinar matrix and to increase RANKL
42 as an activator of osteoclasts *Kovacs (2001)*. During lactation, RANKL targets
43 osteoclasts, thereby driving osteoclastic bone resorption. Osteocytic osteolysis is
44 accomplished through the expression of 'osteoclast-specific' genes such as cathepsin
45 K (*Ctsk*), tartrate-resistant acid phosphatase (TRAP, gene *Acp5*), and carbonic
46 anhydrase 1 (*Car 1*) *Qing and Bonewald (2009)*; *Qing et al. (2012)*. In addition, there
47 is an increase in genes coding for the proton pumps, ATPase H⁺ Transporting V1
48 Subunit G1 (*Atp6v1g1*) and ATPase H⁺ Transporting V0 Subunit D2 (*Atp6v0d2*)
49 necessary to dissolve and remove calcium from bone collagen *Jahn (2017)*.

50 Systemic calcium deficiency such as a decrease in dietary calcium triggers
51 an increase in PTH, acting to mobilize calcium from bones to maintain normal
52 homeostatic circulating calcium *Goltzman (2008)*. Worldwide, over 3.5 billion people
53 suffer from dietary calcium deficiency, and women are at a higher risk of this
54 condition *Kumssa et al. (2015)*; *Body et al. (2016)*. Aging often results in
55 hypocalcemia and bone loss due to low vitamin D, hypoparathyroidism, genetic
56 abnormalities, medications decreasing dietary calcium absorption, and menopause
57 in women. Calcium deficiency can lead to osteopenia, osteoporosis, and increased
58 fracture risk, primarily due to secondary hyperparathyroidism *Kumssa et al. (2015)*;
59 *Body et al. (2016)*.

60 Irisin is a recently discovered myokine generated in response to exercise when
61 Fibronectin type III Domain Containing protein 5 (FNDC5) is proteolytically cleaved by a
62 yet undetermined protease *Bostrom et al. (2012)*. FNDC5 is expressed in the heart,
63 kidney, testes, brain, and other tissues; however, skeletal muscle appears to be the
64 primary producer *Erickson (2013)*; *Maak et al. (2021)*; *Tsourdi et al. (2022)*. Cleaved
65 irisin circulates to distant organs, such as adipose tissue where irisin increases a
66 thermogenic gene program, including the expression of uncoupling protein 1 (UCP1)
67 in a process referred to as browning. This is associated with increased energy
68 expenditure and improvement in glucose tolerance, both of which are important for
69 the prevention of Type 2 diabetes and the reduction of complications from obesity
70 *Perakakis et al. (2017)*; *Korta et al. (2019)*. Irisin can also regulate glucose uptake
71 in skeletal muscle *Lee et al. (2015)*, and increases myogenesis and oxidative
72 metabolism, responsible for increasing skeletal muscle mass *Colaianni and Grano*

73 (2015). Irisin also plays an important positive role in cognitive functions with
74 exercise, aging, and degenerative diseases such as Alzheimer's disease (AD) and
75 Parkinson's disease (PD) *Islam et al. (2021)*. Using the tail-vein injection method to
76 deliver exogenous irisin, it was shown that irisin can cross the blood-brain barrier
77 *Islam et al. (2021)*.

78 Results from studies regarding the effects of irisin on the skeleton are
79 complex and somewhat contradictory. Colaianni et al have shown that recombinant
80 irisin exerts a beneficial effect on cortical bone in young male mice by reducing the
81 secretion of osteoblast inhibitors and increasing the activity of osteogenic cells
82 *Colaianni et al. (2015)*. However, another study has shown that recombinant irisin
83 treatment of MLO-Y4 osteocyte-like cells induces gene and protein level expression of
84 *Sost/sclerostin*, a negative regulator of bone formation while maintaining cell viability
85 under oxidative stress *Kim et al. (2018)*. Rosen et al. have shown using female
86 FNDC5 overexpressing female mice that irisin acts directly acts on osteoclast
87 progenitors to increase differentiation and promote bone resorption *Estell et al.*
88 *(2020)*. Kim et al. have shown that 9-month-old ovariectomized FNDC5 global KO
89 mice are protected against ovariectomy-induced trabecular bone loss through the
90 inactivation of osteocytic osteolysis and osteoclastic bone resorption *Kim et al.*
91 *(2018)*. The majority of these studies used only male or female mice, suggesting a
92 sex-dependent response may be responsible for these seemingly opposing findings
93 *Estell et al. (2020)*; *Colaianni et al. (2017)*; *Kawao et al. (2018)*; *Ma et al. (2018)*;
94 *Colucci et al. (2019)*; *Posa et al. (2021)*.

95 As shown previously, FNDC5 deletion has a protective effect against ovariectomy-
96 induced bone loss via a reduction of osteocytic osteolysis and osteoclastic resorption *Kim*
97 *et al. (2018)*. We, therefore, hypothesized that FNDC5 deletion would also be
98 protective against bone loss due to calcium deficiency that occurs with lactation and
99 a calcium-deficient diet. Our data show that the female skeleton in FNDC5 null
100 female mice was resistant to bone loss due to both lactation and low calcium.
101 However, for FNDC5 null males, deletion not only failed to protect but exacerbated
102 bone loss in response to low calcium. We propose that male and female osteocytes
103 respond to irisin differently under calcium-demanding conditions based on the
104 divergence of the male and female osteocyte transcriptome with sexual maturity
105 when the female osteocyte must serve a critical role in reproduction and lactation.

106

Results

With lactation, FNDC5 global KO mice lose less bone and are mechanically stronger compared to WT

No significant differences were observed in either bone composition or morphometry between 4-5-month-old virgin WT and FNDC5 global KO female mice (Fig 1A, 1B, 1C, sup table 1), showing that the absence of FNDC5/irisin does not affect female bone development. It has been previously shown that during lactation, maternal bones release calcium to supplement milk, especially in response to the large calcium demand induced by large litter size or a calcium-deficient diet *Wysolmerski (2002); Ardeshirpour et al. (2015)*. Similar to previous studies, 2 weeks of lactation resulted in bone loss in both WT and KO mice, with a significant reduction in cortical bone area (Ct. B.Ar), cortical bone area fraction percentage (Ct.B.Ar/T.Ar%), and cortical thickness (Ct. Th) (Fig 1A, 1B) as well as bone mineral density, BMD (Fig 1C). However, the KO mice lost less bone compared to the WT mice, as evidenced by the significantly higher bone area fraction percent, cortical thickness, and BMD (Fig. 1A, 1B, 1C) as well as the lower percentage of bone loss (Sup Table 1). These data suggest that the FNDC5 KO mice are more resistant to the effects of calcium demand. Analysis of trabecular bone parameters including trabecular bone volume fraction (BV/TV), trabecular thickness (Tb. Th), trabecular spacing (Tb. Sp), and trabecular number (Tb. N) showed no significant difference in bone loss between lactating WT and lactating KO mice (Sup table 1). There was no significant difference in the pup numbers between WT and KO females (Sup fig 1A).

Bone loss can have significant effects on bone mechanical properties including bone strength, stiffness, and fragility. To determine mechanical properties, 3-point bending tests were performed on mice femurs. There was no significant difference between virgin WT and KO mice in terms of ultimate force and stiffness (Fig. 1D). However, femurs from the lactating KO mice were stronger than lactating WT, as evidenced by the higher stiffness and significantly higher ultimate force needed to break the bone (Fig 1D, Sup Table 1, Table 2). This data indicates that lactating KO female bone retains greater resistance to fracture than lactating WT mice.

139 With lactation, FNDC5 global KO mice have fewer TRAP-
140 positive osteoclasts and osteocytes as well as smaller osteocyte
141 lacunar area compared to WT mice

142 Previously it was shown that lactation-induced bone loss occurs via not only
143 osteoclastic bone resorption but also osteocytic osteolysis *Qing et al (2012)*. To
144 determine the relative contribution of each means of resorption, tibial longitudinal
145 sections were stained for tartrate-resistant acid phosphatase TRAP-positive
146 multinucleated osteoclasts as well as TRAP-positive osteocytes.

147 Virgin FNDC5 KO female mice had fewer TRAP-positive osteocytes
148 compared to virgin WT mice (Fig. 1E, 1G). This is the first and only difference we have
149 observed between WT and KO female mice and suggests that the osteocytes in the
150 female KO mice are less ‘primed’ to initiate osteocytic osteolysis. With lactation, TRAP-
151 positive osteocytes significantly increased in both WT and KO mice (Fig 1G, Sup Table
152 2). Virgin KO mice started with a lower number of TRAP- positive osteocytes compared
153 to virgin WT, and with lactation, their number of TRAP-positive osteocytes was still
154 significantly lower compared to lactating WT (Fig. 1G).

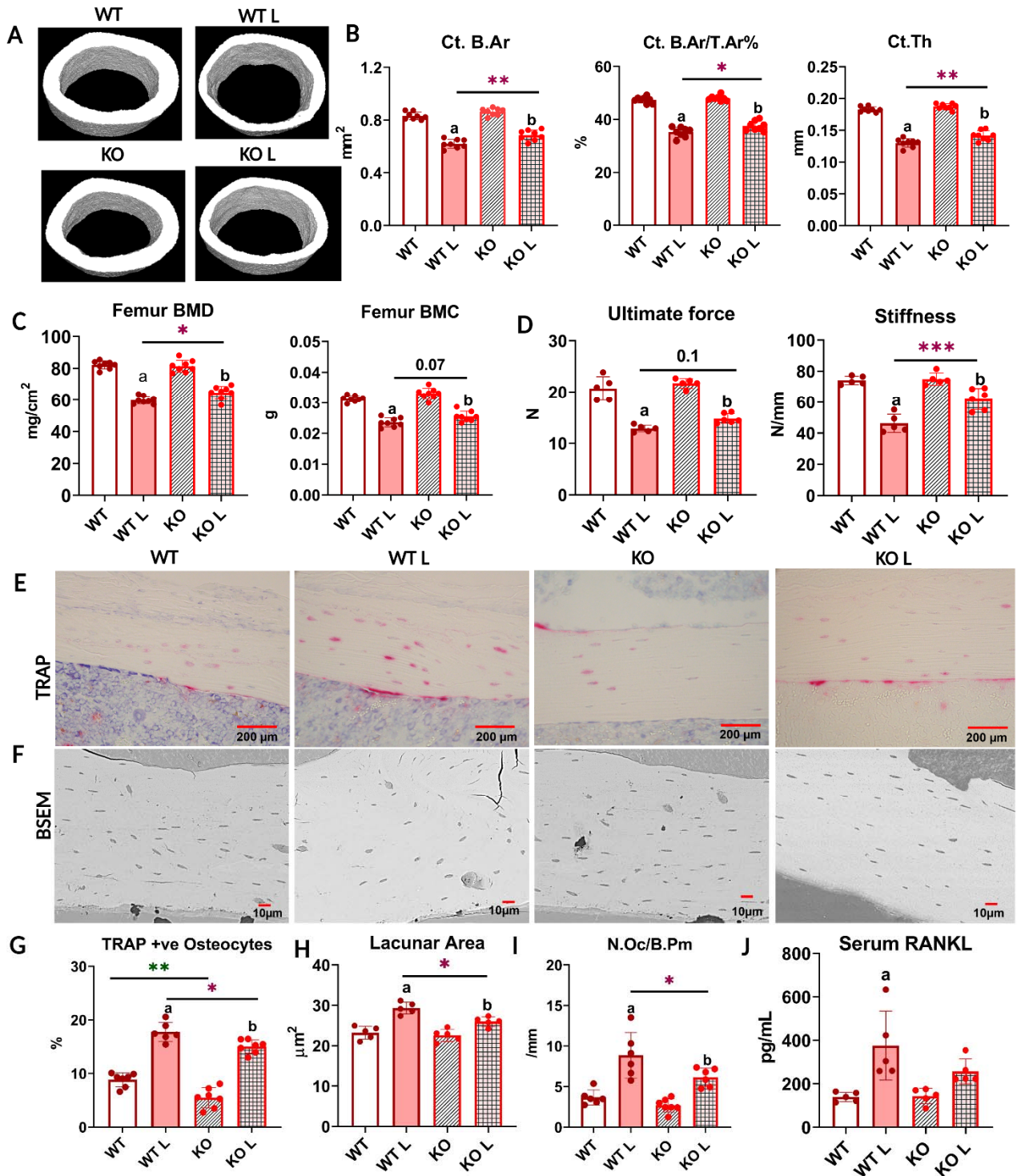
155 During lactation, in response to calcium demand, osteocytes can remove their
156 perilacunar matrix. This process is similar but not identical to osteoclastic bone
157 resorption *Tsourdi et al. (2018)*; *Bélangier (1969)*; *Wysolmerski (2012)* as
158 osteoclasts generate resorption pits, whereas osteocytes increase their lacunar size
159 *Qing et al. (2012)*; *Wysolmerski (2013)*. We measured the osteocyte lacunar area
160 and found no significant difference between virgin WT and KO female mice (Fig. 1F,
161 1H) even though the KO females have fewer TRAP-positive osteocytes (Fig. 1G).
162 With lactation, the lacunar area increased in both groups; however, KO mice had
163 significantly smaller average lacunar area compared to WT (Fig. 1H). These data
164 show that female lactating FNDC5 KO mice undergo less osteocytic osteolysis
165 compared to WT females under the calcium-demanding condition of lactation.

166 In virgin mice, there were no significant differences in osteoclast number per
167 bone perimeter (Oc/B.Pm) between WT and KO female mice (Fig 1I). With lactation,
168 osteoclast number increased in both groups, however, KO mice had significantly
169 fewer osteoclasts (Fig 1I) and a significantly lower percentage increase in the
170 number of osteoclasts compared to WT (Sup Table 1). This suggests that with
171 lactation, fewer osteoclasts are activated in the KO as compared to the WT mice.

172 RANKL, another major factor in bone resorption *Xiong and O’Brien (2012)*,
173 is also increased during lactation to induce osteoclastic bone resorption

174
175
176
177
178

Ardeshirpour et al. (2015) by osteocytes, the major source of RANKL *Nakashima et al. (2011)*; *Xiong and O'Brien (2012)*; *Ono et al. (2020)*. Virgin WT and KO mice had comparable serum RANKL levels (Fig. 1J). With lactation, the increase in serum RANKL was significant in the WT mice, but not in the KO mice (Fig. 1I, Sup Table 1).



179

180 **Fig 1: With lactation, FNDC5 global KO mice lose less bone and are mechanically**
181 **stronger compared to WT**

182 **A:** Respective μ CT images of femoral midshafts from WT virgin (WT), KO virgin
183 (KO), WT lactation (WT L), and KO lactation (KO L) mice.

184 **B:** μ CT analysis of femoral cortical bone parameters of virgin and lactating WT
185 and KO female mice reported as cortical bone area (Ct. B.Ar), cortical bone area
186 fraction (Ct. B.Ar/ T.Ar %), and cortical thickness (Ct. Th).

187 **C:** Ex vivo DXA analysis for BMD and BMC of femurs from virgin and lactating
188 WT and KO female mice.

189 **D:** 3-point bending analysis of WT and KO virgin and lactating mice reported
190 as ultimate force and stiffness.

191 **E:** Representative TRAP-stained images of cortical bone from WT virgin (WT),
192 WT lactation (WT L), KO virgin (KO), and KO lactation (KO L) mice.

193 **F:** Representative backscatter scanning electron microscope (BSEM) images of
194 WT virgin (WT), KO virgin (KO), WT lactation (WT L), and KO lactation (KO L) mice
195 femur at 400X magnification.

196 **G:** Percent TRAP-positive osteocytes (TRAP +ve) in tibia from virgin and
197 lactating WT and KO mice.

198 **H:** Average osteocyte lacunar area in femurs from virgin and lactating WT and
199 mice.

200 **I:** Osteoclast number per bone perimeter in tibia from virgin and lactating WT
201 and KO mice.

202 **J:** Serum RANKL levels in virgin and lactating WT and KO mice.

203 4-5-month-old WT and KO virgin and lactating mice, n= 5-8/group. a=
204 Significantly different from WT, b= Significantly different from KO, *= p< 0.05, **= p<
205 0.01, ***= p< 0.001. 2-way ANOVA was performed for statistical analysis.

207 **FNDC5 KO female and male bone have opposite responses**
208 **to a low- calcium diet**

209 After observing that bones are protected against lactation-induced bone loss
210 in FNDC5/irisin KO female mice, we sought to determine if FNDC5/irisin null (KO)
211 male bone is protected from calcium deficiency. Therefore, both female and male
212 mice were placed on a calcium-deficient diet for 2 weeks to induce bone loss.

213 With regards to the female mice, similar results were observed with the low

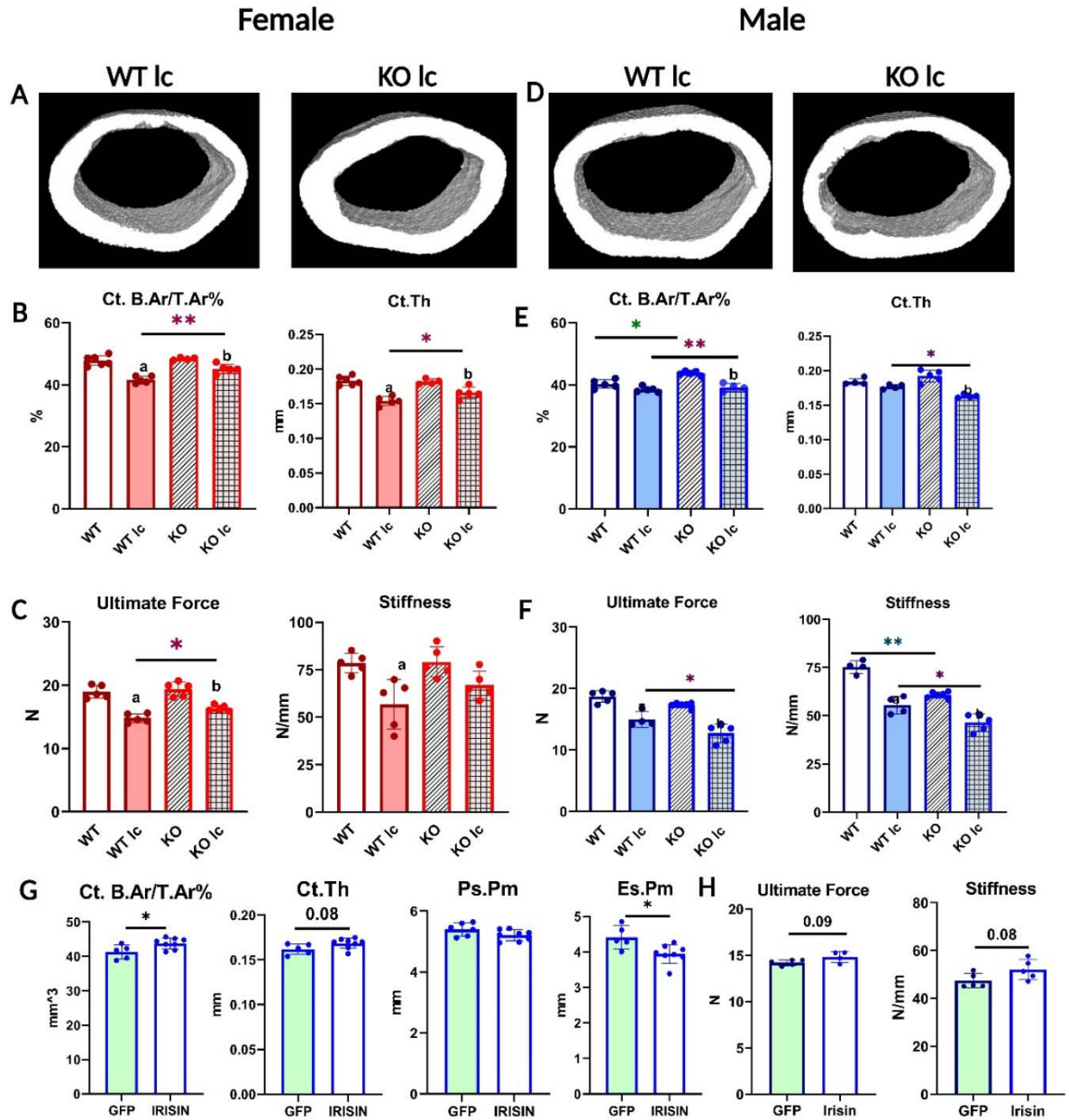
214 calcium diet as was observed with lactation. At baseline, WT and KO female mice
215 showed no significant differences in their BMD and BMC (Sup Table 2), as well as no
216 differences in either cortical (Fig 2B) or trabecular bone parameters (Sup Table 3).
217 After 2 weeks on a low calcium diet, both WT and KO female mice lost bone as can
218 be evidenced by decreased BMD (Sup Table 2) and bone area fraction (Fig 2B).
219 However, similar to the lactation experiment, the KO female mice were partially
220 resistant to bone loss compared to the female WT mice given a low calcium diet (Fig
221 2A, B). Interestingly a higher marrow cavity area was observed in the WT compared to
222 the KO, unlike the lactation experiment (Sup Table 2). Mechanical testing showed
223 that bone from female KO mice required a significantly higher force to break, and
224 thus were stronger compared to WT females given a low calcium diet (Fig 2C).
225 Therefore, similar to the calcium-demanding conditions of lactation, on a low calcium
226 diet, the female KO bones are more resistant to bone loss than WT.

227 Unlike female bone, significant differences were observed between WT and
228 KO male bone at baseline. KO male mice on a normal diet had a significantly higher
229 BMD, BMC (Sup Table 2), and bone area fraction compared to WT males of the
230 same age (Fig 2E). However, femurs from KO mice had significantly lower stiffness
231 than WT (Fig 2F), indicating a difference in the material properties of the bone.
232 Therefore, the KO males have larger, denser, but weaker bones compared to WT
233 males. To determine the effect of calcium deficiency on male mice, KO and WT
234 mice were subjected to a low-calcium diet for 2 weeks. Unlike the female KO mice
235 which were protected from the effects of a low calcium diet, the KO male mice had
236 an opposite response. The male KO mice had greater bone loss compared to the
237 WT male mice (Fig 2D, E, Table 2), the trabecular bone loss followed the same
238 trends but was not statistically significant (Sup Table 2), and the femurs from the KO
239 male mice were significantly less stiff and therefore weaker compared to the WT
240 males on a low calcium diet (Fig 2F). These data confirm a sex-specific response to
241 a low calcium diet.

242 To ensure that the effects observed in the KO mice were due to circulating
243 irisin, and not FNDC5 deletion, we injected AAV8- irisin in KO male mice, with
244 AAV8-GFP as the control, and placed them on the same low Ca diet. We chose
245 male mice due to the highly significant effect on bone strength we saw in the KO
246 males compared to WT males on a low-calcium diet. The irisin injection rescued the
247 skeletal phenotype in KO male mice, shown by the higher cortical bone area fraction
248 and the lower endosteal perimeter (Fig 2G). There was a tendency for higher ultimate
249 force and stiffness in the KO males that received the AAV8-irisin injection, however,
250 this did not reach statistical significance (Fig 2H). These data show that the observed

251

effects in the FNDC5 null animals are due to an absence of irisin.



252

253

Fig 2: FNDC5 KO female and male mice have opposite responses to a low-calcium diet with regard to bone composition, structure, and mechanics, and irisin injection rescues FNDC5 KO male mice phenotype under a low-calcium diet

254

A: Representative μ CT images of femoral midshaft cortical bones from WT low-calcium diet female mouse (WT lc) and KO low-calcium diet female mouse (KO lc).

255

256

B: Female femoral midshaft cortical bone parameters of WT control (WT), WT low-calcium diet (WT lc), KO control (KO), and KO low-calcium diet (KO lc) mice reported as cortical bone area fraction (Ct. B.Ar/T.Ar%) and cortical thickness (Ct.Th).

257

258

259

260

261 **C:** Mechanical properties of femurs from female WT and KO control and low- calcium
262 diet reported as ultimate force and stiffness.

263 **D:** Representative μ CT images of femoral midshaft cortical bones from WT low-calcium
264 diet male mice (WT lc) and KO low-calcium diet male mice (KO lc).

265 **E:** Male femoral midshaft cortical bone parameters of WT control (WT), WT low-calcium
266 diet (WT lc), KO control (KO), and KO low-calcium diet (KO lc) mice reported as cortical bone
267 area fraction (Ct. B.Ar/T.Ar%) and cortical thickness (Ct. Th).

268 **F:** Mechanical properties of femurs from male WT and KO control and low- calcium diet
269 reported as ultimate force and stiffness.

270 n= 4-5/group. a= Significantly different from WT, b= Significantly different from KO, *= p<
271 0.05, **= p< 0.01. 2-way ANOVA was performed. As depicted here, red is female, and blue is
272 male.

273 **G:** μ CT measurement of femoral cortical bone of AAV8-GFP or AAV8-irisin injected male
274 KO mice after a 2-week low calcium diet, reported as cortical bone area fraction (Ct.
275 B.Ar/T.Ar%), cortical thickness (Ct. Th), periosteal parameter (Ps.Pm), and endosteal parameter
276 (Es.Pm).

277 **H.** Mechanical properties of femurs from male KO low-calcium diet mice injected with
278 AAV8-GFP or AAV8-irisin reported as ultimate force and stiffness.

279 n= 5-7/group, *= p< 0.05. Student's t-test was performed for statistical analysis between
280 male KO GFP vs irisin-injected mice. As depicted here, green shaded bars represent GFP-
281 injected mice.

283 Osteocytes from female and male KO mice respond 284 differently to a low- calcium diet

285 To investigate if the bone loss was due to osteoclast or osteocyte activation,
286 tibiae from all the groups were TRAP-stained. Under a normal control diet, the tibia
287 from both KO female and male (Fig. 3A) mice had fewer TRAP-positive osteocytes
288 compared to their WT counterparts. This indicates that their osteocytes were less
289 'primed' or 'activated' for resorption. Under a low calcium diet, the number of TRAP-
290 positive osteocytes increased in both WT and KO female mice, similar to lactation (Fig
291 3A, Table 1); however, the total number was still significantly lower in the KO females
292 than the WT females. The low calcium diet increased TRAP-positive osteocytes in both
293 WT and KO male mice. The KO male mice had a significantly higher level of increase
294 (Fig 3A, Table 1), and had significantly more TRAP-positive osteocytes compared to

295 WT. This indicates an increased activation of osteocytes in the KO males and suggests
296 higher osteocytic bone resorption.

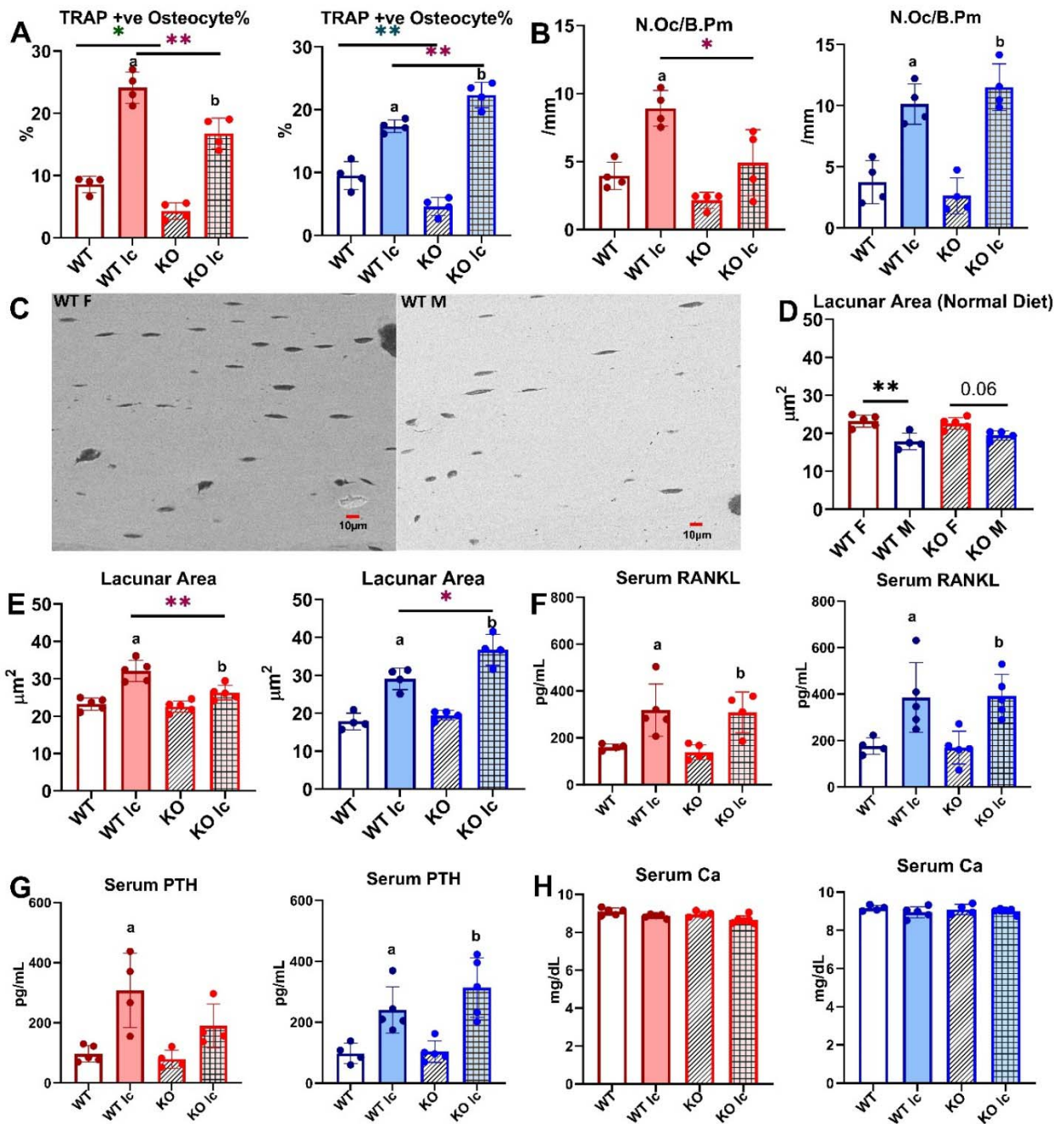
297 There was no significant difference between WT and KO mice in osteoclast
298 numbers per bone perimeter for both females and males (Fig. 3B). Both WT and KO
299 females had an increase in their multinucleated TRAP-positive osteoclast number with
300 a low-calcium diet, however, KO females had a significantly lower number of
301 osteoclasts compared to WT females on a low-calcium diet (Fig 3B). Similarly, under a
302 normal diet, there was no difference in the number of osteoclasts between male WT
303 and KO. Under a low-calcium diet, osteoclast numbers increased in both groups,
304 however, there was no significant difference between WT and KO male mice (Fig. 3B).
305 We also measured osteoblast numbers per bone perimeter. There was no difference in
306 osteoblast numbers in either female or male normal or low-calcium diet mice (data not
307 shown).

308 Under normal control diet conditions, female WT mice had significantly higher
309 osteocyte lacunar area compared to WT males (Fig 3C, 3D). There was no
310 significant difference between FNDC5 KO female and male mice with regards to
311 osteocyte lacunar area. This indicates that under control conditions, female
312 osteocytes have more resorptive activity. On a low calcium diet, all the groups have
313 increased osteocyte lacunar area, indicating an increased level of osteocytic
314 osteolysis (Fig 3E). However, in female KO mice, the average lacunar area is
315 significantly less than in WT female mice, similar to what was observed with the
316 lactation response. The male KO mice, on the other hand, have significantly larger
317 lacunar areas compared to WT males on a low calcium diet, suggesting increased
318 osteocytic osteolysis. Together these data show that bones from female KO mice
319 are more resistant to calcium-demanding conditions, but the deletion of
320 FNDC5/irisin from males makes them more susceptible to bone loss under calcium-
321 demanding conditions. This also shows that male and female KO mice respond
322 completely differently to the challenge of calcium deficiency.

323 Serum RANKL levels increased in all the low calcium diet groups compared to
324 control diet groups (Fig 3F). There was no significant difference between WT and KO
325 female mice and between WT and KO male mice. Serum PTH was measured
326 because decreases in serum calcium stimulate the parathyroid gland to release PTH to
327 remove calcium from bone to maintain normal calcium levels *Jahn et al (2017)*;
328 *Matikainen et al (2021)*. PTH levels significantly increased in WT females and WT and
329 KO males when subjected to a low calcium diet compared to the control diet (Fig 3G),
330 however, the KO female group did not have a statistically significant increase in PTH
331 levels. There was no significant difference in serum calcium levels in any of the groups

332 (8-10 mg/dL range for all groups), which indicates that the elevated PTH is maintaining
333 normal circulating calcium levels in these mice (Fig 3H).

334 Since irisin is robustly produced in skeletal muscle, we wanted to determine if
335 the deletion of irisin affects muscle function, under either a normal or a low calcium
336 diet. *In vivo* and *ex vivo* muscle contractility functions were performed in these mice.
337 No difference was found between WT and KO mice on either a normal or a low
338 calcium diet (Sup Fig 2). This indicates deletion of FNDC5 is not affecting muscle
339 function and that bone resorption is releasing sufficient calcium into the circulation
340 to maintain calcium homeostasis and supplying sufficient calcium for skeletal
341 muscle function.



342
343 **Fig 3: Osteocytes from female and male KO mice respond**
344 **differently to a low-calcium diet**

345 **A:** Percentage of TRAP-positive (+ve) osteocytes in female and male WT and
346 KO mice given a normal or a low-calcium diet.

347 **B.** Osteoclast number (N.Oc/B.Pm) in WT and KO female and male mice given
348 a normal or a low-calcium diet.

349 **C:** Representative BSEM images depicting osteocyte lacunar area in femurs

350 from WT female (WT F) and WT male (WT M) given a normal diet at 450X
351 magnification.

352 **D:** Osteocyte lacunar area in WT and KO female and male mice given a normal
353 diet.

354 **E:** Lacunar area in female and male WT and KO mice given a normal or a low-
355 calcium diet.

356 **F:** Serum RANKL levels in female and male WT and KO mice given either a
357 normal diet or a low-calcium diet.

358 **G:** Serum PTH levels in female and male WT and KO mice given either a normal
359 diet or a low-calcium diet.

360 **H:** Serum calcium levels in female and male WT and KO mice given either a
361 normal diet or a low-calcium diet.

362 n= 4-5/group. a= Significantly different from WT, b= Significantly different from KO, *= p< 0.05,
363 **= p< 0.01. 2-way ANOVA was performed. As depicted here, red is female, and blue is male.

364

Table 1: Bone Parameters and Serum Markers	Change	% Change in female		% Change in male	
		WT	KO	WT	KO
Bone Area	Decrease	13%	7% *	2%	13% *
Bone Area Fraction	Decrease	17%	11% *	7%	23% *
Cortical Thickness	Decrease	19%	13% *	4%	15% *
Osteoclast Number/ Bone Perimeter	Increase	125%	127%	170%	336% *
TRAP-positive Osteocytes	Increase	180%	290% *	85%	388% *
Osteocyte Lacunar Area	Increase	38%	16% *	60%	89% *
Serum PTH	Increase	150%	75% *	70%	164% *
Serum RANKL	Increase	100%	118%	119%	130%

365 **Table 1: FNDC5 KO female and male mice have opposite responses to a low-**
366 **calcium diet compared to WT female and male mice where female KO mice are protected**
367 **but male KO mice have greater bone loss than WT.** Percentage changes in different bone
368 and serum parameters of WT and KO female and male mice with a 2-week low-calcium diet. *=
369 p<0.05 compared to WT.

Female and male osteocyte transcriptomes are distinctly different

Total RNA sequencing of osteocyte-enriched bone chips from female and male WT mice revealed significant sex-dependent differences in the osteocyte transcriptome under normal conditions (Fig. 4A, C, F). The major differentially expressed genes were involved in the steroid, fatty acid, cholesterol, lipid transport, and metabolic processes. Compared to male WT mice, female WT mice had an approximately 2-3-fold higher expression of very low-density lipoprotein receptor (*Vldlr*), voltage-dependent calcium channel T type alpha 1H subunit (*Cacna1h*), aldehyde dehydrogenase (*Aldh1l2*), and a 2-3-fold lower expression of apolipoproteins *Apoa1*, *Apoa2*, *Apoa4*, *Apoc3* and others involved in steroid and fatty acid metabolic process. There was also a 2-3-fold lower expression of several lipid and solute carrier genes and apolipoprotein genes in female WT compared to male WT. This suggests that male osteocytes may be greater regulators and utilizers of these sources of energy than female osteocytes.

Differences were also observed in genes involved in extracellular matrix organization pathways, bone development, ossification, bone remodeling, and resorption pathways. Female WT osteocytes have higher expression of genes shown to be highly expressed in osteocytes during lactation compared to male WT osteocytes. These include *Tnfsf11* (RANKL, 2.7-fold), *Ctsk* (2.5-fold), *Acp5* (TRAP, 2.2-fold), *Mmp13* (2.7-fold), osteoclast associated receptor (*Oscar*, 4.6-fold), macrophage stimulating 1 receptor (*Mst1r*, 3-fold), as well as several collagen genes and bone formation and mineralization genes including alkaline phosphatase (*Alpl*, 2.4-fold), periostin (*Postn*, 2.6-fold), and *Dmp1* (2.2-fold). *TGFβ3* was expressed higher in the WT females compared to WT males, but no significant difference was found in either *TGFβ1* or *TGFβ2* expression levels between WT females and males. This suggests that the higher expression of bone formation genes may be to accommodate the rapid replacement of the perilacunar matrix with weaning. The upregulated and downregulated pathways in WT females compared to WT males are depicted in Fig. 4.

399

400

401

402

Female and male KO osteocyte transcriptomes have fewer differences compared to WT female and male transcriptomes

403

404

405

406

407

408

409

410

411

KO female and KO male osteocyte transcriptomes significantly differed in pathways facilitating ossification and bone mineralization, and extracellular structure and matrix organization (Fig. 4B, F). In KO females, several collagen genes such as *Col2a1*, *Col5a2*, *Col8a2*, and *Col11a1* were 2-4-fold greater compared to KO males. Bone formation genes including *Alpl* (2.5-fold), osteocalcin (*Bglap*, 2.7-fold), *Postn* (2.9-fold), and *Wnt4* (2.4-fold) were also more highly expressed in KO females compared to KO males, however, the resorption genes including *Acp5* and *Ctsk* were not significantly different between KO female and KO male osteocytes. *TGFβ3* was higher in the KO females compared to KO males, similar to the WTs.

412

413

414

415

416

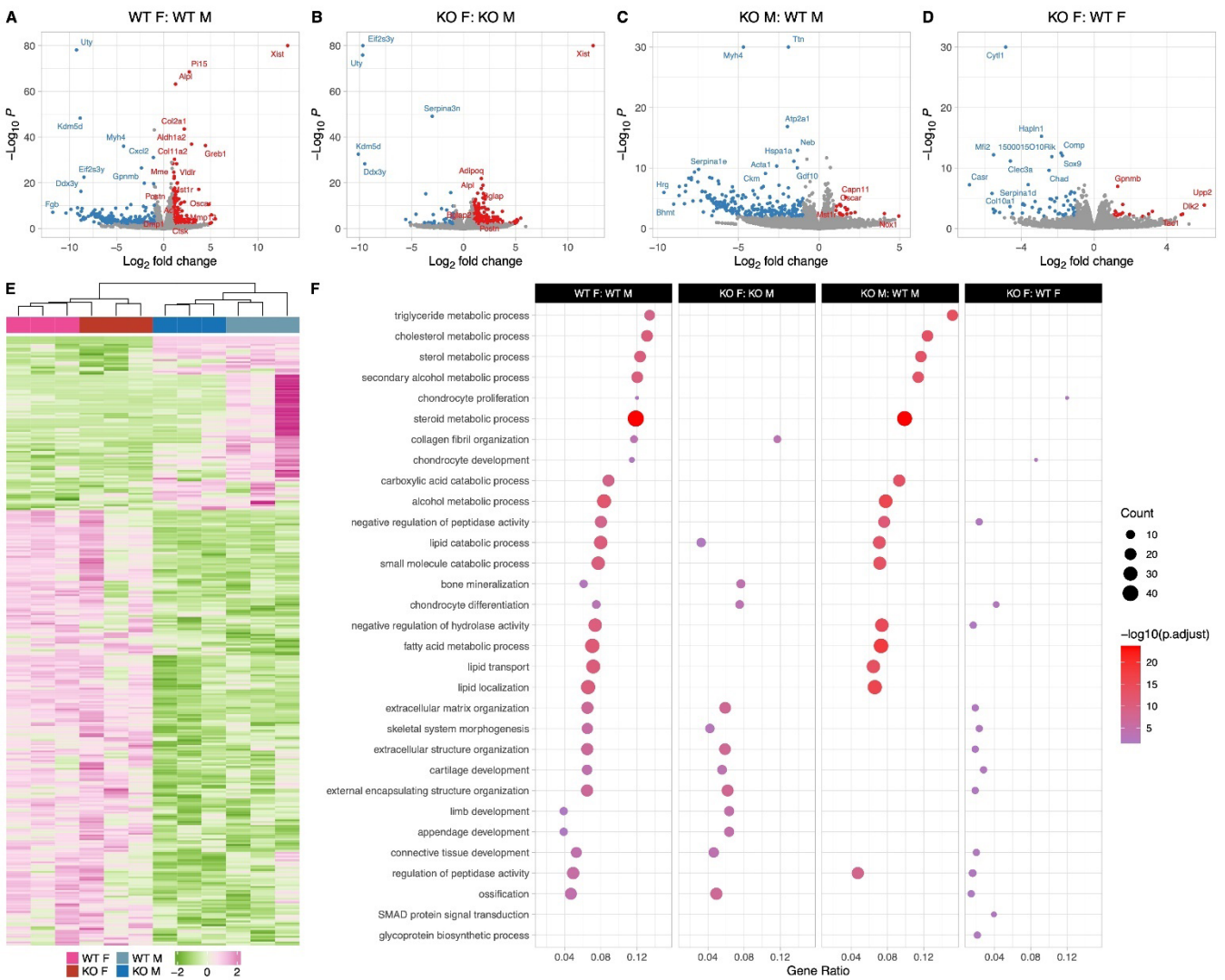
417

418

419

420

The transcriptomes of WT and KO male osteocytes differed significantly, with much lower expression of genes in pathways involving steroid, fatty acid, lipid, and cholesterol transport and metabolic processes in the KO males compared to WT males (Fig. 4C, F). A 2-4-fold downregulation of genes coding for solute carriers, aldehyde oxidase, and fatty acid binding proteins was observed in KO males, while *Oscar* and *Mst1r* are 2-3-fold higher in KO males compared to WT males. In contrast, a relatively low number of genes, 40, were differentially expressed between WT female and KO female osteocytes which reflects the lack of differences in bone morphology and bone mechanical properties (Fig. 4D, F).



421

422

423

424

425

426

427

428

429

430

431

432

433

Fig 4: Female and male wildtype osteocyte transcriptomes are distinctly different; however, female and male KO osteocyte transcriptomes have fewer differences compared to WT female and male transcriptomes

A: Volcano plot showing the significantly regulated genes between WT female control (WT F) and WT male control (WT M) osteocyte transcriptome.

B: Volcano plot showing the significantly regulated genes between KO female control (KO F) and KO male control (KO M) osteocyte transcriptome.

C: Volcano plot showing the significantly regulated genes between WT male control (WT M) and KO male control (KO M) osteocyte transcriptome.

D: Volcano plot showing the significantly regulated genes between WT female control (WT F) and KO female control (KO F) osteocyte transcriptome.

434 **E:** Heat map showing the differentially expressed genes among WT female
435 control (WT F), WT male control (WT M), KO female control (KO F), and KO male
436 control (KO M) osteocyte transcriptome.

437 **F:** Gene set enrichment analysis of Gene Ontology (GO) analysis of the
438 significantly regulated genes between WT female control (WT F) and WT male
439 control (WT M) osteocyte transcriptome, between KO female control (KO F) and KO
440 male control (KO M) osteocyte transcriptome, WT male control (WT M) and KO
441 male control (KO M) osteocyte transcriptome, and WT female control (WT F) and KO
442 female control (KO F) osteocyte transcriptome. The figure shows the union of the top
443 10 GO terms of each analysis. If a term in the union, besides the top 10, is also
444 significant (adjusted p-value less than 0.05) in an analysis, it is also included in the
445 figure.

446 In the figure, the first group is compared to the latter or reference group.
447 n=3/group.

448

449 With calcium deficiency, genes responsible for osteocytic 450 osteolysis are lower in the female KO compared to the female 451 WT osteocyte transcriptome

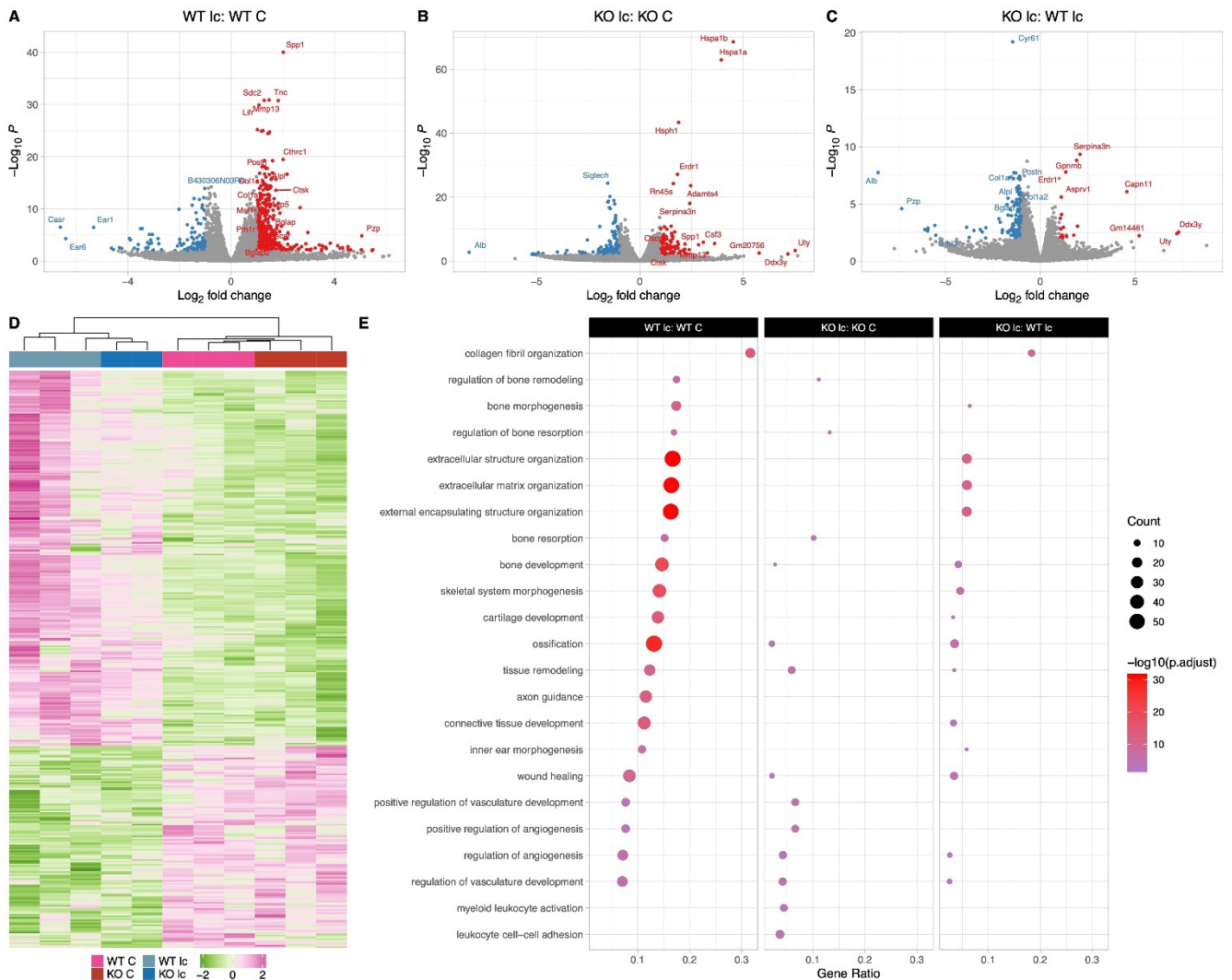
452 Calcium deficiency in WT female mice induced higher expression of
453 osteoclast and resorption genes compared to WT females on a normal diet (Fig. 5A,
454 E). *Acp5*, *Ctsk*, *Pth1r*, and *Mst1r* were elevated 2-4-fold in the calcium-deficient WT
455 females. Real-time PCR analysis of osteocytes also showed an increase in *Tnfrsf11*,
456 *Acp5*, and *Ctsk* gene expression levels in the calcium-deficient WT females compared
457 to WT females on a normal diet. There was no difference in *Sost* expression (Sup Fig
458 2D). Additionally, 5 different *Mmps* (*Mmp13*, *Mmp15*, *Mmp2*, *Mmp16*, and *Mmp14*)
459 were upregulated 2-3.5-fold in the WT calcium-deficient females. These are genes
460 thought to play a role in osteocytic osteolysis. Bone formation and remodeling genes
461 including *Bglap*, *Bglap2*, *Alpl*, *Wnt 5a*, and *Wnt 2b* were upregulated 2-5-fold in the WT
462 low calcium diet group compared to WT female normal diet group as well. These genes
463 may be increased to provide quick bone formation upon return to normal calcium
464 demand.

465 Calcium deficiency in KO female mice also induced increased expression of a
466 number of osteoclast and resorption genes including *Ctsk* (2.8-fold), *Mmp13* (3- fold),
467 and *Oscar* (2.6-fold) in comparison to KO female osteocytes on a normal diet (Fig. 5B,

468
469
470
471
472
473
474
475
476
477
478
479
480
481
482

E). However, unlike the WT osteocytes, expression of *Acp5* and *Pth1r* were not different in osteocytes from KO female mice on a normal diet or a low calcium diet. Real-time PCR analysis also showed an increase in *Ctsk* gene expression level in the calcium-deficient KO females compared to KO females on a normal diet, with no significant difference in the expression levels of *Tnfsf11*, *Acp5*, and *Sost* genes (Sup fig 2D).

Next, we compared KO female mice on a low-calcium diet to WT female mice on a low-calcium diet (Fig. 5C, E). Several bone resorption genes were lower by 2-fold in KO females, including *Tnfsf11* and *Mmp15*. Real-time PCR analysis also showed a significantly lower expression of the *Tnfsf11* gene in the calcium-deficient KO females compared to calcium-deficient WT females (Sup Fig 2D). Additionally, bone formation genes including *Alpl*, *Bglap*, *Wnt2b*, *Col1a1*, *Col1a2*, and *Postn* were also approximately 2-fold lower in the KO low calcium females compared to WT low calcium females. This suggests that female KO osteocytes are less responsive to calcium deficiency than female WT osteocytes.



483

Fig 5: The Osteocyte transcriptomes from female WT and KO mice are distinct when challenged with a low-calcium diet

A: Volcano plot showing the significantly regulated genes between WT female control (WT C) and WT female low-calcium diet-fed mice (WT lc) osteocyte transcriptome.

B: Volcano plot showing the significantly regulated genes between KO female control (KO C) and KO female low-calcium diet-fed mice (KO lc) osteocyte transcriptome.

C: Volcano plot showing the significantly regulated genes between WT female low-calcium diet-fed mice (WT lc) and KO female low-calcium diet-fed mice (KO lc) osteocyte transcriptome.

D: Heat map showing the differentially expressed genes among WT female control (WT C), WT female low-calcium diet-fed mice (WT lc), KO female control (KO C), and KO female low-calcium diet-fed mice (KO lc) osteocyte transcriptome.

E: Gene set enrichment analysis of Gene Ontology (GO) analysis of the significantly regulated genes between WT female control (WT C) and WT female low-calcium diet-fed mice (WT lc) osteocyte transcriptome, between KO female control (KO C) and KO female low-calcium diet-fed mice (KO lc) osteocyte transcriptome, and WT female low-calcium diet-fed mice (WT lc) and KO female low-calcium diet-fed mice (KO lc) osteocyte transcriptome. The figure shows the union of the top 10 GO terms of each analysis. If a term in the union, besides the top 10, is also significant (adjusted p-value less than 0.05) in an analysis, it is also included in the figure.

In the figure, the first group is compared to the latter or reference group. n=2-3/group.

With calcium deficiency, genes responsible for bone resorption, bone formation, and lipid metabolism are differentially regulated in the osteocyte transcriptome in male KO mice compared to male WT mice

Calcium deficiency in WT male mice caused a 2-7-fold increased expression of *Tnfrsf11*, *Acp5*, *Ctsk*, *Oscar*, and *Mst1r* in their osteocyte transcriptome compared to WT males on a normal diet (Fig. 6A, E). Real-time PCR validation also showed a

517 similar increase in *Tnfs11*, *Acp5*, and *Ctsk* gene expression levels in the calcium-
518 deficient WT males compared to WT males on a normal diet (Sup Fig 2E). Bone
519 formation and remodeling genes including *Postn*, *Col1a1*, *Col1a2*, *Bglap*, and *Wnt4*
520 were also elevated 2-4-fold in the WT male low calcium diet compared to the WT
521 normal diet control group.

522 Multiple genes involved in the steroid and fatty acid metabolic process
523 pathways as well as lipid catabolic processes were downregulated 2-7-fold in the
524 calcium-deficient WT males compared to WT males on a normal diet. These genes
525 include several solute carrier family protein genes *Slc27a2* and *Slc27a5*, several
526 apolipoprotein genes including *Apoa1*, *ApoB*, and *Apoc1*, several cyp genes
527 including *Cyp2e1* and *Cyp7a1*, and *Plin1*.

528 Similarly, osteocytes from KO males on a low calcium diet had a 2-4-fold higher
529 expression of osteoclast genes such as *Tnfs11*, *Oscar*, and *Car3* and a 2-5-fold
530 upregulation of bone formation genes such as *Col1a1*, *Col1a2*, *Alpl*, *Bglap*, and *Postn*
531 compared to osteocytes from KO males on a normal diet (Fig. 6B, E). Therefore,
532 genes responsible for bone resorption and bone formation are increased in both WT
533 and KO with calcium deficiency. Real-time PCR data showed an increase in
534 *Tnfs11*, *Acp5*, and *Ctsk* gene expression levels in the calcium-deficient KO males
535 compared to KO males on a normal diet, validating the RNA sequencing data (Sup
536 Fig 2E).

537 When KO males were compared to WT males on a low calcium diet (Fig. 6C,
538 E), there was a 2-3-fold higher expression of bone resorption genes including *Oscar*
539 and *Mst1r* in the KO low calcium diet males compared to WTs. Several collagen
540 formation genes and ossification genes including *Col3a1*, *Col8a2*, *Tnn*, *Aspn*, and
541 *Igf1* were also significantly downregulated in the KO males on a low-calcium diet
542 compared to WTs on a low-calcium diet. It is not clear whether these also play a role in
543 the increased bone resorption observed with calcium deficiency in KO males. Real-time
544 PCR analysis showed no significant difference in expression levels of *Tnfs11*, *Acp5*,
545 *Sost*, and *Ctsk* genes between calcium-deficient KO males and calcium-deficient WT
546 males, reflecting the RNA sequencing data (Sup Fig 2E). No significant difference was
547 observed in expression levels of genes involved in the lipid catabolic process pathway
548 or fatty acid metabolism pathways.



549

550

551

Fig 6: The Osteocyte transcriptomes from male WT and KO mice are distinct when challenged with a low-calcium diet

552

A: Volcano plot showing the significantly regulated genes between WT male control (WT C) and WT male low-calcium diet-fed mice (WT Ic) osteocyte transcriptome.

555

B: Volcano plot showing the significantly regulated genes between KO male control (KO C) and KO male low-calcium diet-fed mice (KO Ic) osteocyte transcriptome.

557

C: Volcano plot showing the significantly regulated genes between WT male low-calcium diet-fed mice (WT Ic) and KO male low-calcium diet-fed mice (KO Ic) osteocyte transcriptome.

560

D: Heat map showing the differentially expressed genes among WT male control (WT C), WT male low-calcium diet-fed mice (WT Ic), KO female control (KO C), and KO male low-calcium diet-fed mice (KO Ic) osteocyte transcriptome.

562

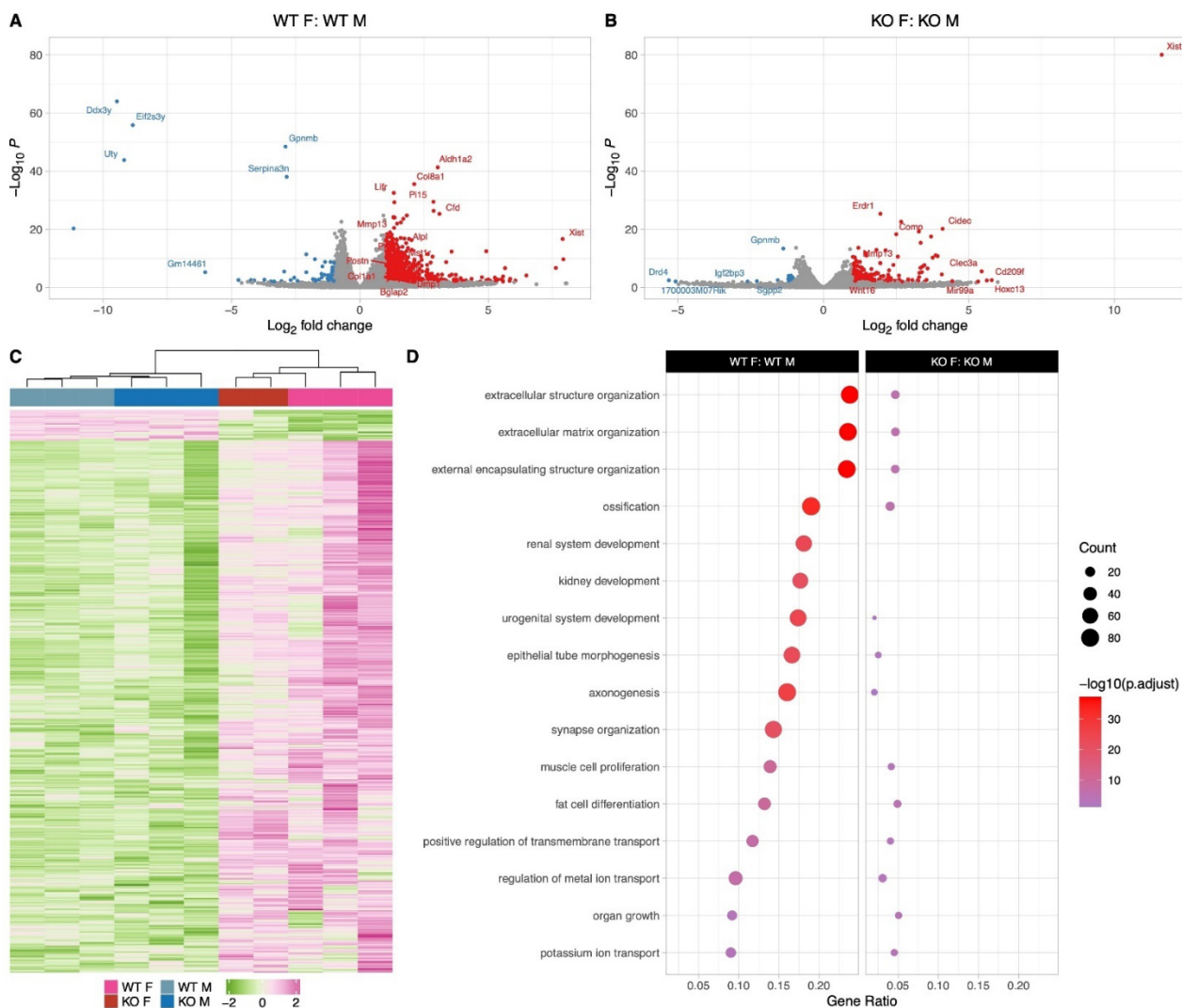
563 **E:** Gene set enrichment analysis of Gene Ontology (GO) analysis of the
564 significantly regulated genes between WT male control (WT C) and WT male low-
565 calcium diet-fed mice (WT lc) osteocyte transcriptome, between KO male control (KO
566 C) and KO male low-calcium diet-fed mice (KO lc) osteocyte transcriptome, and WT
567 male low-calcium diet-fed mice (WT lc) and KO male low-calcium diet-fed mice (KO
568 lc) osteocyte transcriptome. The figure shows the union of the top 10 GO terms of
569 each analysis. If a term in the union, besides the top 10, is also significant (adjusted
570 p-value less than 0.05) in an analysis, it is also included in the figure.

571 In the figure, the first group is compared to the latter or reference group.
572 n=3/group.

574 Male and female osteocytes respond differently to calcium 575 deficiency in a genotype-specific manner

576 In response to 2 weeks of calcium deficiency, WT female mice had higher
577 expression of genes involved in extracellular matrix and structure organization as
578 well as ossification compared to WT male mice with calcium deficiency. Calcium
579 deficiency in WT female mice caused significantly increased expression of bone
580 formation genes compared to WT males including several collagen genes such as
581 *Col2a1*, *Col6a3*, *Col4a2*, as well as *Postn*, and *Bglap2*. This was accompanied by
582 an increased expression of bone resorbing genes in WT females including several
583 *Car* genes, *Mmp13*, *Mmp16*, *Tnfsf11*, and *Mst1r* compared to WT males on a low-
584 calcium diet (Fig. 7A, C, D). This suggests that both bone formation and bone
585 resorption are upregulated in WT females compared to WT males in response to
586 calcium deficiency, and WT females undergo higher bone remodeling compared to
587 WT males.

588 On the other hand, in response to calcium deficiency, KO female and KO
589 male mice have fewer significantly differentially expressed genes compared to WT
590 females and WT males (Fig. 7B, C, D). The main upregulated bone formation
591 genes in KO females compared to KO males include several collagen genes such
592 as *Col2a1* and *Col8a2*. The main bone resorption genes that were upregulated in
593 KO females compared to KO males were *Mmp13* and *Dcstamp*.



594
595 **Fig 7: The Osteocyte transcriptomes from male and**
596 **female mice are distinct when challenged with a low calcium**
597 **diet**

598 **A:** Volcano plot showing the significantly regulated genes between WT female
599 low-calcium diet-fed (WT F) and WT male low-calcium diet-fed mice (WT M) osteocyte
600 transcriptome.

601 **B:** Volcano plot showing the significantly regulated genes between KO female
602 low-calcium diet-fed (KO F) and KO male low-calcium diet-fed mice (KO M) osteocyte
603 transcriptome.

604 **C:** Heat map showing the differentially expressed genes among WT male low-
605 calcium diet-fed mice (WT M), KO male low-calcium diet-fed mice (KO M), WT female
606 low-calcium diet-fed (WT F), and KO female low-calcium diet-fed (KO F) osteocyte
607 transcriptome.

608 **D:** Gene set enrichment analysis of Gene Ontology (GO) analysis of the
609 significantly regulated genes between WT female low-calcium diet-fed (WT F) and
610 WT male low-calcium diet-fed mice (WT M) osteocyte transcriptome, and between KO
611 female low-calcium diet-fed (KO F) and KO male low-calcium diet-fed mice (KO M)
612 osteocyte transcriptome. The figure shows the union of the top 10 GO terms of
613 each analysis. If a term in the union, besides the top 10, is also significant (adjusted
614 p-value less than 0.05) in an analysis, it is also included in the figure.

615 In the figure, the first group is compared to the latter or reference group. n=2-
616 3/group.

617

Discussion

618
619 Irisin has been shown to be increased in the blood of humans and mice with
620 exercise. Irisin, working mainly through its receptor $\alpha V\beta 5$ integrin, has been shown to
621 have powerful effects on fat, bone, and brain tissues *Bostrom et al. (2012)*; *Tsourdi et*
622 *al. (2022)*; *Korta et al. (2019)*; *Islam et al. (2021)*; *Kim et al. (2018)*; *Colaianne et*
623 *al. (2017)*; *Wrann et al. (2013)*; *Xin et al (2016)*; *Wang et al. (2017)*; *Bao et al.*
624 *(2022)*; *Zhang et al. (2022)*. With regard to bone, studies have generated complex and
625 even contradictory results *Erickson (2013)*; *Maak et al. (2021)*; *Colaianne and Grano*
626 *(2015)*; *Kim et al. (2018)*; *Estell et al. (2020)*; *Colaianne et al. (2014)*; *Zhang et al.*
627 *(2018)*. Of note, the majority of bone studies have been performed either exclusively on
628 males, or females, but few on both. Most studies have used recombinant irisin
629 treatment whereas we have focused on the effects of deleting irisin. Other studies have
630 mainly examined the effects on osteoblasts and osteoclasts, whereas our studies have
631 focused on osteocytes *Kim et al. (2018)*.

632 Global deletion of FNDC5 on a normal diet had essentially no effect on bone
633 in females, but in contrast, the null male mice have significantly more bone compared
634 to wildtype males, but this bone has impaired mechanical properties. This suggests
635 that the lack of FNDC5 is having no effect on the development or growth of the
636 female skeleton, but does affect the male skeleton, increasing the size yet impairing
637 matrix properties responsible for strength. Examination of their osteocytes showed
638 that both female and male null mice have significantly fewer TRAP-positive
639 osteocytes compared to their sex-matched wildtype controls suggesting that their
640 osteocytes are more quiescent or less primed for bone resorption.

641 Challenging the null animals with calcium deficiency revealed dramatic
642 differences in osteocytic osteolysis and osteoclast activation, two major functions of
643 osteocytes. Deletion of FNDC5 in females is partially protective against calcium
644 deficiency, but deletion in males accelerates both of these osteocyte functions
645 resulting in greater bone loss compared to controls. We have shown previously that
646 under calcium-demanding conditions such as lactation, osteocytes express genes
647 previously thought only to be specific for osteoclasts including cathepsin K, TRAP,
648 carbonic anhydrase, the proton pump V-ATPase, and others *Qing et al. (2012)* and
649 shown that osteocytes are the major source of RANKL *Nakashima et al. (2011)*;
650 *Xiong and O'Brien (2012)*; *Xiong et al. (2015)*. In this study, lactating females
651 lacking FNDC5 were partially resistant to bone loss, similar to ovariectomized
652 females as previously published *Kim et al. (2018)*. To determine the effects of
653 calcium deficiency on males, mice were given a low-calcium diet for 2 weeks. Unlike

654 the protective effects of FNDC5/irisin deletion in females, bone loss was
655 exacerbated in null males compared to controls on a low calcium diet.

656 With two weeks of lactation and litter size comparable to wildtype controls,
657 the null female mice had less circulating RANKL, fewer TRAP-positive osteoclasts,
658 fewer TRAP-positive osteocytes, and smaller lacunar size. Our observation that the
659 deletion of FNDC5/irisin makes lactating mice partially resistant to bone loss has an
660 important implication with regard to the purpose of lactation. Lactation is a critical
661 period for pups as they obtain essential nutrients, especially calcium, from the
662 mother's milk for their proper growth. Calcium lost by the mother's bone during
663 lactation is rapidly replaced upon weaning with complete recovery of bone mass within
664 a week *Qing et al. (2012)*; *Wysolmerski (2002)*; *Kalkwarf (2004)*; *Kovacs (2001)*;
665 *Wysolmerski (2012)*. Our data suggest that irisin acts as a regulator of calcium release
666 from maternal bones to fulfill the offspring demands during lactation. Therefore, irisin
667 appears to play a beneficial role in ensuring offspring survival and consequently,
668 successful reproduction.

669 To determine if low calcium would have a similar effect on male FNDC5 null
670 bone, both males and females were subjected to a low-calcium diet for 2 weeks. The
671 effects of a low-calcium diet on female osteocytes and bone loss were essentially
672 identical to the effects of lactation, with two exceptions. First, serum RANKL levels were
673 not significantly different between virgin and lactating null females, while they were
674 between null females on a normal compared to a calcium diet suggesting that RANKL
675 plays less of a role in lactation compared to calcium deficiency. Secondly, the
676 medullary cavity and endosteal bone in the low-calcium females were completely
677 protected in the FNDC5 null females but were not in the lactating FNDC5 null mice.
678 Bone loss due to lactation or due to dietary calcium deficiency may target different bone
679 sites. Our unpublished observations suggest that endosteal bone is removed faster
680 than periosteal bone with lactation, but this remains to be carefully validated. This
681 difference may also be due to elevated PTHrP during lactation *Kovacs (2001)*,
682 whereas hypocalcemia increases circulating PTH levels *Goltzman (2008)*, and it is not
683 clear if hormones target distinct bone sites. Similar to the lactating FNDC5 null mice,
684 the null females placed on the low calcium diet had fewer TRAP-positive osteoclasts,
685 fewer TRAP-positive osteocytes, and smaller lacunar size. Serum RANKL levels
686 increased in both wildtype and null mice with dietary calcium deficiency, therefore,
687 serum RANKL alone is not enough to explain the partial protective effect of FNDC5
688 deletion against bone loss. In summary, female null mice are not only resistant to
689 bone loss due to estrogen deficiency as we showed previously *Kim (2018)* but are

690 also resistant to calcium deficiency either due to an increase in PTHrP as with
691 lactation, or an increase in PTH as with a low calcium diet.

692 Osteoporosis manifests earlier in females due to menopause, but males also
693 develop osteoporosis but at an older age *Johannesdottir et al. (2013)*; *Johnston*
694 *and Dagar (2020)*, and the elderly are known to suffer from calcium deficiency which
695 accelerates bone loss *Kumssa et al. (2015)*; *Body et al. (2016)*. Dietary calcium
696 deficiency has been shown previously to affect female and male bone differently
697 where female rat bones are more sensitive to a low calcium diet compared to males
698 *Geng and Wright (2001)*. Similarly, in our study, we saw that wildtype females
699 were more affected by calcium deficiency and lost more bone compared to wildtype
700 male mice. However, the opposite was observed for the FNDC5/irisin null mice,
701 where female null mice were partially resistant, and male null mice were more
702 susceptible to bone loss with calcium deficiency compared to their wildtype
703 counterparts. Despite starting with more bone volume compared to wildtype, the
704 FNDC5 null males had increased osteocyte lacunar area and lost more bone with
705 dietary calcium deficiency compared to wild-type males. This greater bone loss can
706 be explained through the dramatic increase of TRAP-positive osteocytes and TRAP-
707 positive osteoclasts, but not by a significantly greater increase in circulating RANKL.
708 This sex difference indicates that FNDC5/irisin may be involved in the regulation of
709 calcium release from bone via osteocytes in a sex-dependent manner.

710 Lacunar area is an indicator of osteocyte regulation of their lacunar
711 microenvironment. Here we report that osteocyte lacunar size is significantly larger in
712 virgin wildtype female mice compared to same-age wildtype males. This difference in
713 lacunar area indicates a distinction between female and male osteocyte function.
714 The mammalian skeleton is a sexually dimorphic organ *Sharma (2023)*, and female
715 and male bones respond differently to circulating factors, hormones, and myokines as
716 well as other challenges *Kurapaty and Hsu (2022)*; *Lu et al. (2022)*; *Osipov et al.*
717 *(2022)*. As osteocytes are regulators of bone formation and resorption *Bonewald*
718 *(2011)*; *Dallas et al. (2013)*; *Robling and Bonewald (2020)*, this sex difference may
719 be due to differences in male and female osteocytes. A recent study by Youtlen
720 and colleagues has shown that male and female osteocyte transcriptomes are
721 distinctly different *Youtlen et al. (2021)*. At 4 weeks of age, the female osteocyte
722 transcriptome diverges from the male osteocyte transcriptome and these differences
723 continue with age. A cluster of genes more highly expressed in female osteocytes
724 compared to male osteocytes are those involved in bone resorption, the same ones
725 elevated in osteocytes in response to lactation. These transcripts include genes

726 necessary for osteocytic perilacunar remodeling and reduction in pH, which are
727 essential for calcium removal *Qing et al. (2012)*. This suggests that the larger
728 lacunar area in female osteocytes compared to male osteocytes may be due to the
729 higher expression of bone resorption genes.

730 The magnitude of the effect size due to FNDC5 deficiency appears modest
731 with regards to the quantitative cortical bone parameters. However, if one
732 examines the changes in osteocyte lacunar size and the mechanical properties of
733 these bones, the differences are greater. As shown in Figure 3 E, the lacunar area
734 of the wildtype females on a low calcium diet increases by over 30% and the
735 FNDC5-null by less than 20%, while in the males it is approximately 38% in
736 wildtype compared to 46% in null. According to Sims and Buenzli *Buenzli and*
737 *Sims (2015)*, a potential total loss of ~16,000 mm³ (16 mL) of bone occurs through
738 lactation in the human skeleton. This was based on our measurements in lactation-
739 induced murine osteocytic osteolysis *Qing et al. (2012)*. They used our 2D section
740 of tibiae from lactating mice showing an increase in lacunar size from 38 to 46 μm².
741 In that paper we also showed that canalicular width is increased with lactation.
742 Therefore, this suggests dramatically lower intracortical porosity due to the
743 osteocyte lacunocanalicular system in female null mice compared to female wild-
744 type mice either with lactation or a low calcium diet and a dramatic increase in
745 intracortical porosity in null males compared to wild-type males on a low calcium
746 diet. Based on these data, using the FNDC5 null animals, we would speculate that
747 the product of FNDC5, irisin, is having a significant effect on the ultrastructure of
748 bone in both males and females challenged with a low calcium diet.

749 To begin to understand the molecular mechanisms responsible for the sex
750 and genotype differences, we compared the osteocyte transcriptomes of 5-month-old
751 female and male, wildtype and null mice. Our results show that the osteocyte
752 transcriptomes of female and male wildtype mice are significantly different under
753 normal conditions. A surprising difference we observed but not described in the
754 Youtlen paper *Youtlen et al. (2021)* was that compared to wildtype female
755 osteocytes, wildtype male osteocytes have much higher expression of genes
756 involved in steroid, lipid, and cholesterol metabolism and transport pathways, lipid
757 and solute carrier genes, and apolipoprotein genes. This suggests that osteocyte
758 metabolism and bioenergetics are distinctly different between wildtype females and
759 wildtype males. We hypothesize that the differentially expressed genes in these
760 bioenergetic and metabolic pathways modulate bone mass and formation and may
761 shed light on the sexual dimorphism of bones. As these differentially regulated

762 pathways were not previously reported by Youtlen and colleagues *Youtlen et al.*
763 (2021), this may be due to differences in strain, housing, diet, or microbiome.
764 Another explanation is the greater osteocyte purity in our study as we used a series of
765 collagenase digestions and EDTA chelation to remove any surface cells which was
766 not performed in the Youtlen paper *Youtlen et al. (2021)*.

767 A second major difference between female and male wildtype osteocytes was
768 the higher expression of genes involved in collagen matrix formation, bone
769 mineralization, remodeling, resorption, and osteocytic osteolysis pathways in females
770 compared to males. Many of the highly expressed bone resorption genes in wildtype
771 female osteocytes have been shown to be elevated during lactation *Qing et al.*
772 (2012) including *Acp5*, *Ctsk*, and *Mmp13*, all involved in osteocytic osteolysis. This
773 further supports our hypothesis that wildtype female osteocytes are more primed for
774 resorption compared to wildtype males, presumably to meet the increased calcium
775 demand during lactation, and correlates with the observed larger lacunae compared
776 to males.

777 TGF β is another potential player in osteocyte perilacunar/canalicular
778 remodeling. Alliston and colleagues generated transgenic mice with reduced
779 expression of the TGF β Type II receptor in mice expressing *Dmp1-Cre* *Dole et al.*
780 (2020) (PMID: 32282961) and found a significant difference in bone parameters
781 and markers of osteocyte perilacunar remodeling between the sexes. The females
782 were subjected to lactation and the transgenics were found to be resistant to
783 osteocytic osteolysis compared to controls. However, these investigators did not
784 investigate the lacunar remodeling process in males as compared to females as
785 was performed in the present study using a low calcium diet. Their study does
786 suggest that TGF β is involved in the osteocytic osteolysis that occurs with lactation,
787 however, even though the transgenic males showed a disrupted lacunocanalicular
788 network compared to wildtype males, this does not necessarily indicate a defect in
789 perilacunar remodeling. It is more likely that the defect occurred during bone
790 formation when osteoblasts were differentiating into osteocytes. In our study, we
791 observed a higher expression of *TGF β 3* in wildtype female mice compared to
792 wildtype male mice, with no significant differences in *TGF β 1* or *TGF β 2* expression.
793 This suggests that *TGF β 3* may play a role in generating the larger lacunar area in
794 wildtype females compared to wildtype males.

795 Few differences were observed between wildtype female and null female
796 osteocyte transcriptomes as would be expected for bone morphometry and the only
797 difference observed was the number of TRAP-positive osteocytes. In contrast,

798 osteocytes from wildtype males and null males are significantly different with
799 regards to fatty acid and lipid metabolism pathways whereas null male mice have
800 lower expression of these genes compared to wildtype males. This suggests a role
801 for irisin in lipid metabolism and bioenergetics in male osteocytes. Lower
802 expression in the null male mice may be responsible for the higher bone mass and
803 inferior biomechanical properties compared to wildtype males suggesting these
804 pathways mediate the effects of irisin on male bone.

805 Osteocytes from null females have higher expression of genes and pathways
806 involved in collagen matrix organization, ossification, and mineralization compared
807 to null males. Unlike wildtype males and females, there was no difference in
808 expression of lipid, cholesterol, and fatty acid metabolism genes in null males
809 compared to null females. Again, this indicates that irisin regulates male bone
810 through these lipid-related pathways.

811 Lactation and calcium deficiency induce the same changes in females.
812 Similar to that reported previously for lactation *Qing et al. (2012)*, osteocytes from
813 wildtype female mice on a low calcium diet exhibited an increase of several osteo-
814 clast/resorption/lactation genes including *Acp5*, *Ctsk*, *Oscar*, *Mst1r*, and *Pth1r* compared
815 to wildtype females on a normal diet. Surprisingly, we also observed an increase in
816 bone formation genes including *Col1a1*, *Alpl*, and *Bglap*. As osteocytic osteolysis is
817 rapidly reversed within a week of weaning, the osteocyte may be preparing to rapidly
818 reverse bone loss. We propose that once calcium is replenished, shutting off the proton
819 pump will rapidly reverse the pH within the osteocyte lacunae, allowing bone-forming
820 proteins such as alkaline phosphatase to become active to rapidly replace the
821 osteocyte perilacunar matrix *Jahn et al. (2017)*; *Andersson et al. (2003)*; *Silver et al.*
822 *(1988)*; *Kaplan (1972)*; *Farley and Baylink (1986)*.

823 The main molecular mechanism responsible for the resistance of null female
824 mice to calcium deficiency compared to wildtype female mice is lower expression of
825 genes such as *Tnfsf11*, responsible for osteoclastic resorption. A correspondingly
826 lower expression of bone formation genes including *Col1a1*, *Alpl*, and *Bglap*
827 compared to wildtype females on a low-calcium diet was observed. The lower
828 expression of both formation and resorption genes suggests a coupling of
829 resorption with formation. Irisin appears to regulate calcium release in the female
830 skeleton.

831 Osteocytes from wildtype male mice on a low calcium diet expressed higher
832 levels of bone resorption genes including *Tnfsf11*, *Acp5*, *Ctsk*, *Oscar*, and *Mst1r*
833 compared to wildtype male mice on a normal diet as expected. Like the females,

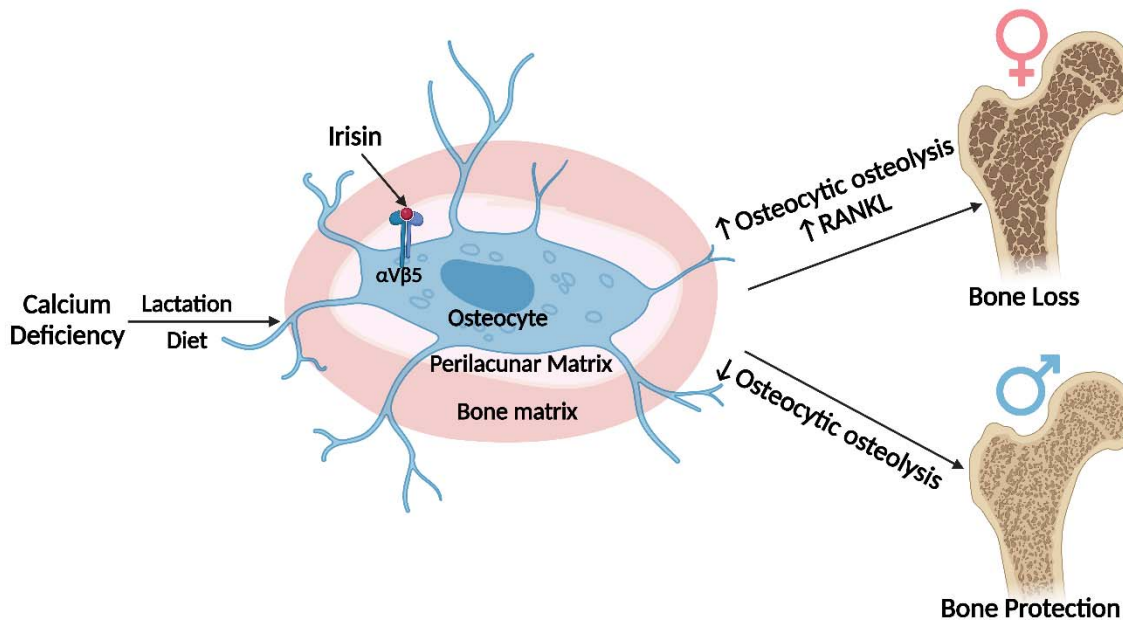
834 there is a coupling with bone formation genes as there is also an increase in *Bglap* and
835 *Col1a1*, suggesting the potential for osteocytes to rapidly replace their perilacunar
836 matrix with calcium repletion. Similarly, the male null mice with calcium deficiency
837 showed an increase in bone resorption genes including *Tnfsf11*, *Oscar*, and *Car3*, as
838 well as an increase in bone formation genes such as *Alpl* and *Bglap* compared to
839 null mice on a normal diet. The major differences between wildtype male mice with
840 calcium deficiency and FNDC5-null male mice with calcium deficiency were the
841 lower expression of genes involved in the extracellular matrix organization,
842 ossification, and bone development pathways in the null male mice compared to
843 wildtype males. This suggests a mechanism for how null male mice lose more bone
844 with calcium deficiency compared to wildtype males.

845 Irisin could be having direct or indirect effects on osteocytes. Irisin can modulate
846 adipose tissue *Bostrom et al. (2012)*; *Zhang et al. (2014)*; *Celi and Brown (2017)*;
847 *Luo et al. (2022)*, can potentially modulate osteogenic differentiation of bone marrow
848 mesenchymal stem cells through $\alpha V\beta 5$ *Zhu et al. (2023)* and bone marrow adipose
849 tissue can modulate bone properties *Yeung et al. (2005)*; *Rosen and Bouxsein*
850 *(2006)*; *Muruganandan and Sinal (2014)*; *Styner et al. (2015)*; *Schwartz et al.*
851 *(2015)*; *During (2020)* as well as osteocyte number and activity *Saedi A et al. (2019,*
852 *2020)*. Irisin can modulate brain activity and signaling *Islam et al. (2021)*; *Wrann et*
853 *al. (2013)*; *Young et al. (2019)*; *Jo and Song (2021)*; *Qi et al (2022)* through BDNF
854 *Wrann et al. (2013)* and BDNF promotes osteogenesis in human bone mesenchymal
855 stem cells *Liu et al. (2018)*. Our data do not show significant expression of *Fndc5* in
856 osteocytes. Studies from our group have found no expression of *Fndc5* in primary
857 osteoblasts and primary osteocytes (transcriptome analysis with a raw count of 8-12),
858 however both skeletal muscle (gastrocnemius) and C2C12 myotubes have high
859 expression of *Fndc5* (transcriptome raw count of 512-1000, unpublished). As such, we
860 postulate that the effect of irisin on osteocytes is not an autocrine effect, but rather due
861 to irisin production by skeletal muscle.

862 Irisin must bind to $\alpha V\beta 5$ integrins to function. Osteocytes express high levels of
863 this receptor which was first discovered using the female MLO-Y4 osteocyte-like cell
864 line *Kim et al. (2018)*. Integrins are usually stable in the cell membrane with a half-life
865 of 12-24 hours *Moreno-Layseca et al. (2019)*. In our RNA sequencing data, we
866 observed a stable expression of both *ITGAV* and *ITGB5*, encoding integrins αV and $\beta 5$
867 respectively, with no differences between either wildtype or null, male or female,
868 calcium replete or calcium deficient mice. Recently it has been published that *Hsp90 α* is
869 necessary to facilitate irisin- $\alpha V\beta 5$ binding *Mu et al. (2023)*. *Hsp90a*, the gene encoding

870 this heat shock protein, is very highly expressed in both wildtype and null male and
871 female mice, with no significant regulation by diet. The high expression of Hsp90 α in
872 osteocytes may explain their significant and rapid responses to irisin *Kim et al (2018)*.

873 In summary, during normal development and on a regular diet, FND C5/irisin
874 deletion has few if any effects on the female skeleton but a significant effect on the
875 male skeleton resulting in more but weaker bone. However, with challenges, such as
876 calcium deficiency, dramatic differences were observed. Our data suggest that irisin
877 activates the osteocyte in females to initiate the removal of their perilacunar matrix
878 and for bone resorption through osteoclast activation, presumably to provide calcium
879 for reproduction purposes. In contrast, in males, irisin protects against osteocytic
880 osteolysis and osteoclastic bone resorption under calcium-demanding conditions.
881 This sex-specific effect may be due to the sexual dimorphism of the osteocyte
882 transcriptome. We have discovered a new novel function of irisin to ensure the
883 survival of offspring and that irisin is essential for male but not female skeletal
884 development. These findings could have implications for understanding sex-
885 dependent differences in bone diseases, such as osteoporosis, and lead to the
886 development of sex- targeted therapies.



887

888 **Fig 8: Graphical abstract** (image was created using BioRender.com)

889 • No differences are observed in bone from Fndc5 /irisin null female,
890 whereas null male skeletons are larger but weaker compared to wildtype controls.

891 • With calcium deficiency, lactating female null mice are protected
892 from bone loss due to osteocytic osteolysis, whereas male null mice on a low calcium diet

893 lose greater amounts of bone compared to their wildtype controls.

894 • The osteocyte transcriptomes show wildtype males have higher
895 expression of the steroid, lipid and fatty acid pathways which are lower in the null males,
896 whereas the wildtype females have higher expression of genes regulating osteocytic
897 osteolysis than null females.

898 • With calcium deficiency, female null osteocytes have lower while
899 male null osteocytes have higher expression of osteocytic osteolysis genes compared to
900 wildtype controls.

901

Methods

Animal Experiments

All animal experiments were performed per procedures approved by the Institutional Animal Care and Use Committee (IACUC) of the Indiana University School of Medicine. Heterozygous C57Bl/6J FNDC5 Knockout (KO) mice were provided by Dr. Bruce Spiegelman at Harvard University and bred in our facility to obtain homozygous global FNDC5 KO and wildtype (WT) control mice. Genotype was determined using a PCR reaction with primers targeting portions of exon 3 absent in KO (WT Forward: GCG GCT CGA GAG ATG AAG AA, WT Reverse: CAG CCC ACA ACA AGA AGT GC, KO Forward: GGA CTT CAA GTC CAA GGT CA, KO Reverse: CCT AAG CCC ACC CAA ATT AC). Mice were housed in a temperature-controlled (20–22°C) room on a 12-hour light/dark cycle with ad libitum food and water. Qualified veterinary staff and/or animal care technicians performed regular health check inspections.

For the lactation experiments, 4-month-old WT and FNDC5 global KO female mice were bred, delivered pups, and lactated for 2 weeks before sacrifice. Virgin WT and KO mice were used as controls. All animals were 4-5 months old at the time of sacrifice and analysis. For all lactating mice, the litter size ranged from 8-11 pups *Qing et al. (2012)*.

For the low calcium diet experiments, 4-5-month-old male and female WT and FNDC5 global KO mice were fed either a control diet (0.6% calcium, Teklad, TD.97191) or a low calcium (Ca) diet (0.01% calcium, 0.4% phosphorus, Teklad TD.95027) for 2 weeks. Distilled water was used in place of tap water to control calcium intake. On the day of sacrifice, blood was collected under anesthesia, and mice were euthanized for sample collection, processing, and analysis *Qing (2012)*; *Jahn et al. (2017)*.

AAV8 injection

AAV8-irisin and AAV8-GFP constructs were obtained from Dr. Bruce Spiegelman at Harvard University. AAV8 Mouse ORF 1-140 (containing the N-terminal signal peptide and irisin) plus a five-amino-acid linker plus a C-terminal flag tag was cloned into the pENN.AAV.CB7.Cl.pm20d1flag.WPRE.rBG vector (Addgene plasmid no. 132682). AAV8-GFP (pENN.AAV.CB7.Cl.eGFP.WPRE.rBG), used as control, was obtained from Addgene (105542), and packaged at the UPenn Vector Core to a titer of 2.10×10^{13} GC per ml³⁹. FNDC5 KO male mice were placed under anesthesia and injected into the tail vein with either AAV8-irisin or AAV8-GFP control (1×10^{10} GC

936 per mouse) in 100 μ L in PBS *Islam et al. (2021)*. One week after injection with either
937 the control virus containing GFP or the virus coding for circulating irisin, the mice
938 were placed on a low-calcium diet for two weeks before sacrifice.

939 *In vivo* and *ex vivo* muscle contractility and 940 electrophysiology measurement

941 *In vivo* plantarflexion torque was assessed one day before sacrifice (Scientific
942 Inc, Canada) as described in *Pin et al. (2022)*. Briefly, the mouse was placed under
943 anesthesia and the left hind foot was affixed to the force transducer aligned with the
944 tibia at 90°. The tibial nerve was stimulated using monopolar electrodes (Natus
945 Neurology, Middleton, WI). Maximum twitch torque was established by using a 0.2 ms
946 square wave pulse. Peak plantarflexion torque was measured by using a stimulation of
947 0.2 ms delivered at 100Hz stimulation frequency.

948 *In vivo* electrophysiological functions were assessed one day before sacrifice
949 with the Sierra Summit 3–12 Channel EMG (Cadwell Laboratories Incorporated,
950 Kennewick, WA, USA) as described in *Huot et al. (2022)*. Briefly, peak-to-peak and
951 baseline-to-peak compound muscle action potentials (CMAP) were measured using
952 supramaximal stimulations of <10 mA continuous current for 0.1 ms duration, and
953 peak-to-peak single motor unit (SMUP) potentials were measured using an
954 incremental stimulation technique. Motor unit number estimation (MUNE) was
955 measured using the equation: MUNE = CMAP amplitude/average SMUP.

956 *Ex vivo* muscle contractility was measured in the extensor digitorum longus
957 (EDL) muscle as described in *Huot et al. (2021)*. EDL was collected from the
958 mouse and mounted between a force transducer, and then submerged in a
959 stimulation bath. The muscles were forced to contract, and data were collected
960 using Dynamic Muscle Control/Data Acquisition (DMC) and Dynamic Muscle Control
961 Data Analysis (DMA) programs (Aurora Scientific). The EDLs were weighed for
962 normalization purposes.

963 Body composition assessment by dual-energy X-ray 964 absorptiometry (DXA)

965 The right femurs from mice were dissected and cleaned of soft tissue, fixed in
966 4% paraformaldehyde (PFA) for 48 hours, and then transferred to 70% ethanol. Ex
967 vivo DXA measurements were obtained using a faxitron (Faxitron X-ray Corp,
968 Wheeling, IL) to measure bone mineral density (BMD) and bone mineral content
969 (BMC) *Essex et al. (2022)*.

Bone morphometry analysis by micro-computed tomography (μ CT)

Right femurs were analyzed using a Skyscan 1176 μ CT as described previously *Pin et al. (2022)*. Briefly, specimens were scanned at 55 kV, 145 μ A, high resolution, 10.5 mm voxel, and 200 ms integration time. For cortical parameters, three-dimensional images from a 1mm region of interest (ROI) of the mid-diaphysis were used to calculate total cortical bone area fraction (Ct. B.Ar/T.Ar%), cortical bone thickness (Ct. Th), marrow cavity area, periosteal perimeter (Ps. Pm), and endosteal perimeter (Es. Pm) according to ASBMR guidelines *Bouxsein et al. (2010)*. For trabecular parameters, three-dimensional images reconstructed within the range of 0.5 mm from the most proximal metaphysis of tibiae were analyzed. Trabecular morphometry was performed by excluding the cortical bone from the endocortical borders using hand-drawn contours followed by thresholding and characterized by bone volume fraction (BV/TV), trabecular number (Tb. N), trabecular thickness (Tb. Th), trabecular spacing (Tb. Sp), and connectivity density (Conn.D) *Kitase et al. (2018)*.

Tartrate-resistant acid phosphatase (TRAP) staining

Tibiae were stripped of soft tissue, fixed in 4% PFA for 48 hours, decalcified in 10% EDTA for 3-4 weeks, and processed into paraffin as described previously followed by sectioning (5 μ m) and staining for TRAP activity using the standard naphthol AS-BI phosphate post coupling method and counterstained with toluidine blue *Pin et al. (2021)*. Briefly, after equilibration in 0.2 M sodium acetate, 50 mM sodium tartrate, pH 5.0, for 20 min at RT, sections were incubated at 37°C in the same buffer containing 0.5 mg/ml naphthol AS-MX phosphate (Sigma Chem. Co., St. Louis, MO) and 1.1 mg/ml Fast Red Violet LB salt (Sigma) and counter-stained in toluidine blue. Images were taken at 5X and 40X using an Olympus BX51 fluorescent microscope and Olympus cellSense Entry 1.2(Build 7533) imaging software. TRAP-positive osteocytes and osteoclasts 1.5 mm distal from the growth plate were quantified using Osteomeasure software (OsteoMetrics.Inc) in a blinded fashion. Toluidine blue-stained osteoblasts from the same sections were quantified 1.5 mm distal from the growth plate using the same software.

Osteocyte lacunar area measurement by Backscatter Scanning Electron Microscopy (BSEM)

Femurs were stripped of soft tissue and fixed in 4% PFA for 48 hours before proceeding to dehydration and embedding steps as previously described *Qing et al. (2012)*. Briefly, femurs were dehydrated in graded ethanol and placed into acetone. Subsequently, the femurs were immersed in infiltration solution made of 85% destabilized methyl methacrylate (MMA, Sigma), 15% dibutyl phthalate (Sigma), 1% PEG400 (Sigma), and 0.7% benzoyl peroxide (Polysciences, Inc., Warrington, PA)/acetone until infiltration was complete. The femurs were then placed on pre-polymerized base layers, covered with freshly catalyzed MMA embedding solution (for 100 mL, 85mL MMA, 14mL dibutyl phthalate, 1mL PEG400, 0.33uL DMT, and 0.8g BPO), and incubated under vacuum until the MMA was polymerized. The polymerized blocks were trimmed, sequentially polished to a completely smooth surface, and coated with gold using a sputter coater (Desk V, Denton Vacuum, NJ, USA). Then BSEM (JEOL: JSM-7800F) was performed to image the osteocyte lacunae on the sectioned bone surface at 450X magnification starting 2 mm distal from the growth plate. Six fields from the endosteal and periosteal sides of the cortical bone were taken as described previously *Qing and Bonewald (2009)*. Using ImageJ (NIH), the images were thresholded for background removal, binarized, and the lacunar area from each sample quantitated.

Mechanical testing using 3-point bending

Mechanical testing was performed essentially as described in *Melville et al. (2015)*. Briefly, the left femurs were stripped of soft tissue, wrapped in PBS- soaked gauze, and stored at -20°C until use. Frozen femurs were brought to room temperature and mounted across the lower supports (8 mm span) of a 3- point bending platen on a TestResources R100 small force testing machine. The samples were tested in monotonic bending to failure using a crosshead speed of 0.05 mm/s. Parameters related to whole bone strength were measured from force/displacement curves.

Serum RANKL analysis

The levels of RANKL were measured in mouse centrifuged serum by using an ELISA kit (Bio-Techne Corporation, Minneapolis, MN), according to the manufacturer's protocol.

1034 Serum parathyroid hormone (PTH) analysis

1035 Serum was obtained from terminal cardiac puncture and serum PTH levels
1036 were determined using the MicroVue Bone Mouse PTH 1-84 ELISA assay (Quidel
1037 Corp., San Diego, CA) according to the manufacturer's protocol.

1038 Calcium measurement

1039 Plasma calcium levels were determined using the Pointe Scientific calcium
1040 Reagent kit (Manufacturer and city). Briefly, diluted serum (1:4 in dH₂O) was
1041 incubated with a working calcium color reagent for 1 min and the absorbance read
1042 at 575 nm using a spectrophotometer (BioTek Synergy HTX).

1043 Sample collection and processing for RNA sequencing

1044 Bulk RNA sequencing was performed on osteocytes from the control and low
1045 calcium diet, male and female, WT and KO mice. Osteocyte RNA was extracted
1046 from tibia and femur diaphyses after sequential digestion to remove surface cells
1047 including osteoclasts, osteoblasts, and lining cells as previously described *Qing et*
1048 *al. (2012)*; *Pin et al. (2022)*. Briefly, soft tissue was removed from the bones, the
1049 epiphyses were cut off and bone marrow was removed by flushing with PBS. The
1050 remaining midshafts were incubated at 37°C with 0.2% type 1 collagenase (Sigma)
1051 for 30 minutes, followed by chelation/ digestion in 0.53 mM EDTA/ 0.05% trypsin
1052 (Cellgro, Mediatech, Inc, Manassas, VA) at 37°C for 30 min followed by a second
1053 collagenase digestion. After each step, the bone chips were rinsed with PBS and
1054 after the final step, flash-frozen in liquid nitrogen, and pulverized in liquid nitrogen,
1055 with Trizol reagent (Qiagen, Carlsbad, CA) added to the resulting bone powder.
1056 Total RNA was isolated with an RNA purification kit (Qiagen miRNeasy mini kit) and
1057 DNase treatment to remove DNA contamination.

1058 Library preparation and RNA sequencing

1059 Total RNA samples were first evaluated for their quantity and quality using
1060 Agilent TapeStation. All the samples used for the sequencing had a RIN of at least 5.
1061 100 nanograms of total RNA were used for library preparation with the KAPA total
1062 RNA Hyperprep Kit (KK8581) (Roche). Each resulting uniquely dual-indexed library
1063 was quantified and quality assessed by Qubit and Agilent TapeStation. Multiple
1064 libraries were pooled in equal molarity. The pooled libraries were sequenced on an
1065 Illumina NovaSeq 6000 sequencer with the v1.5 reagent kit. 100 bp paired-end
1066 reads were generated.

RNA-seq data analysis

The sequencing reads were first quality-checked using FastQC (v0.11.5, Babraham Bioinformatics, Cambridge, UK) for quality control. The sequence data were then mapped to the mouse reference genome mm10 using the RNA-seq aligner STAR (v2.7.10a) *Dobin et al. (2013)* with the following parameter: "--outSAMmapqUnique60". To evaluate the quality of the RNA-seq data, the number of reads that fell into different annotated regions (exonic, intronic, splicing junction, intergenic, promoter, UTR, etc.) of the reference genome was assessed using bamutils *Breese and Liu (2013)*. Uniquely mapped reads were used to quantify the gene level expression employing featureCounts (subread v2.0.3) *Liao et al. (2014)* with the following parameters: "-s 2 -Q 10".

Quality control of samples

During data quality control, one of the KO female control samples (sample 23) was found to have a similar proportion of reads on chromosome Y as in male mice and a very low expression of the gene Xist, typically highly expressed in females (Supplementary Figure 3A, 3B), therefore this sample was excluded from the analysis.

The WT female low-calcium diet samples (samples 16, 17, and 18) had low mapping percentages of 37%, 32%, and 61% respectively. This may be due to bacterial contamination. The two possible methods to process these data are to filter all the possible contaminated reads before alignment or align the reads without filtering. However, filtering the possible contaminated reads before alignment may result in removing some reads from the mouse genome which is similar to the bacterial genome (causing lower gene expression). In contrast, using data without filtering may result in some genes having higher expression levels due to reads from the bacterial genome which are aligned to mice genes. We decided to perform a principal component analysis (PCA) using data without filtering and found that the samples clearly clustered into 4 groups: control male mice, control female mice, low-calcium diet male mice, and low-calcium diet female mice (Supplementary Figure 3C). Within each group, the separation of WT and KO mice is also clear. Due to contamination, samples 16 and 18 were slightly far apart from the others. However, contamination should not have a large global influence on the data as samples 16, 17, and 18 are close to the non-contaminated samples 5 and 6, also in the low-calcium diet female group. Additionally, we validated the data using qPCR with selected genes.

Differentially expressed gene analysis

The read counts matrix was imported to R *Team (2022)* and analyzed with DESeq2 *Love et al. (2014)*. Within DESeq2, read counts data were normalized with median of ratios, and differentially expressed genes (DEGs) were detected after independent filtering. In DEG analysis, we first detected DEGs between different groups. Significant genes were defined as genes with a p-value less than 0.01 and absolute log₂ fold change larger than 1. Gene set enrichment analysis was applied on gene sets from Gene Ontology *resource: enriching a GOLD mine (2021)* using R package clusterProfiler *Wu (2021)*. Several RNA sequencing and pathway figures were prepared with R packages ggplot2 *Wickham (2016)* and ComplexHeatmap *Gu (2022)*. The data was deposited in NCBI GEO database (accession number GSE242445).

Real-time quantitative polymerase chain reaction (qPCR)

Total RNA was reverse transcribed to cDNA using the Verso cDNA Kit (Thermo Fisher Scientific). Transcript levels were measured by real-time PCR (Light Cycler 96; Roche), taking advantage of the TaqMan and Sybr Gene Expression Assay System (Thermo Fisher Scientific). Expression levels for RANKL (*Tnfsf11*, Forward primer: CCG AGC TGG TGA AGA AAT TAG, Reverse: CCC AAA GTA CGT CGC ATC

TTG), Cathepsin K (*Ctsk*, Primer Bank ID: Mm.PT.58.9655974, IDT), TRAP (*Acp5*, Mm.PT.58.5755766, IDT), and sclerostin (*Sost*, Mm00470479_m1, Applied Biosystems) were quantitated. Gene expression was normalized to β -2-microglobulin (*B2m*, Forward: ACA GTT CCA CCC GCC TCA CAT T, Reverse: TAG AAA GAC C A G TCC TTG CTG AAG) levels using the standard $2^{-\Delta\Delta C_t}$ method.

Statistical Analysis

Data are expressed as individual data points. The statistical analysis was done by Prism 8.2 (GraphPad Software, San Diego, CA, USA) and R 4.3.0. When comparing three or more groups with two variables, a two-way analysis of variance (ANOVA) was used. To compare between two groups, the unpaired, two-tailed Student's t-test was used. Differences were considered significant at * $p < 0.05$, ** $p < 0.01$, and *** $p < 0.001$.

ACKNOWLEDGEMENTS:

We would like to thank the Center for Medical Genomics, the Small Animal

1135 Phenotypic Core, and the Histology and Histomorphometry Core at the Indiana
1136 Center for Musculoskeletal Health for help and advice with histological sample
1137 preparation. We would like to thank Dr. Yukiko Kitase, Dr. Eijiro Sakamoto, and
1138 Carrie Zhao for their help and advice with the experiments. This work was
1139 supported by NIH awards P01 AG039355 (to L.F.B).

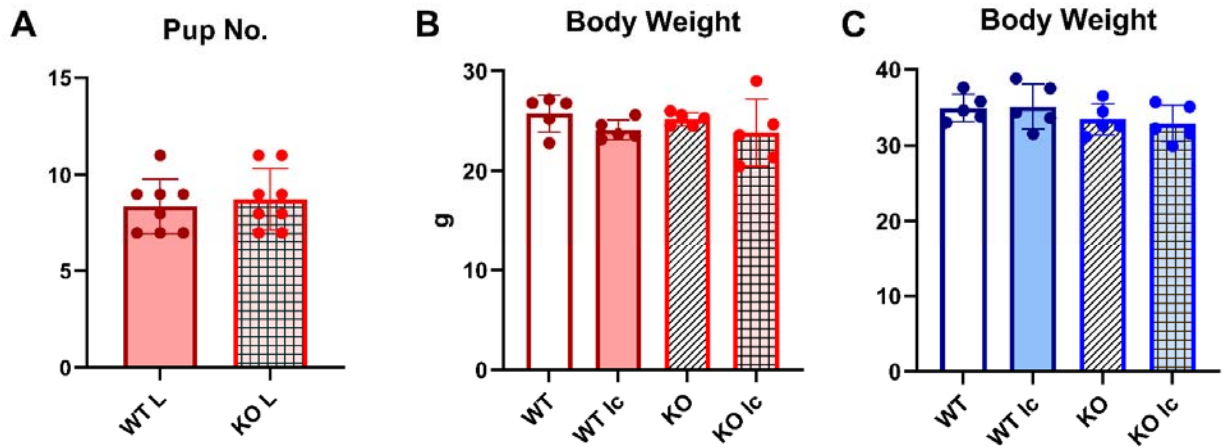
1140 Disclosures

1141 The authors declare that they have no conflicts of interest.

1142 Data Availability Statement

1143 All data that support the findings of this study are available from the
1144 corresponding author upon reasonable request.

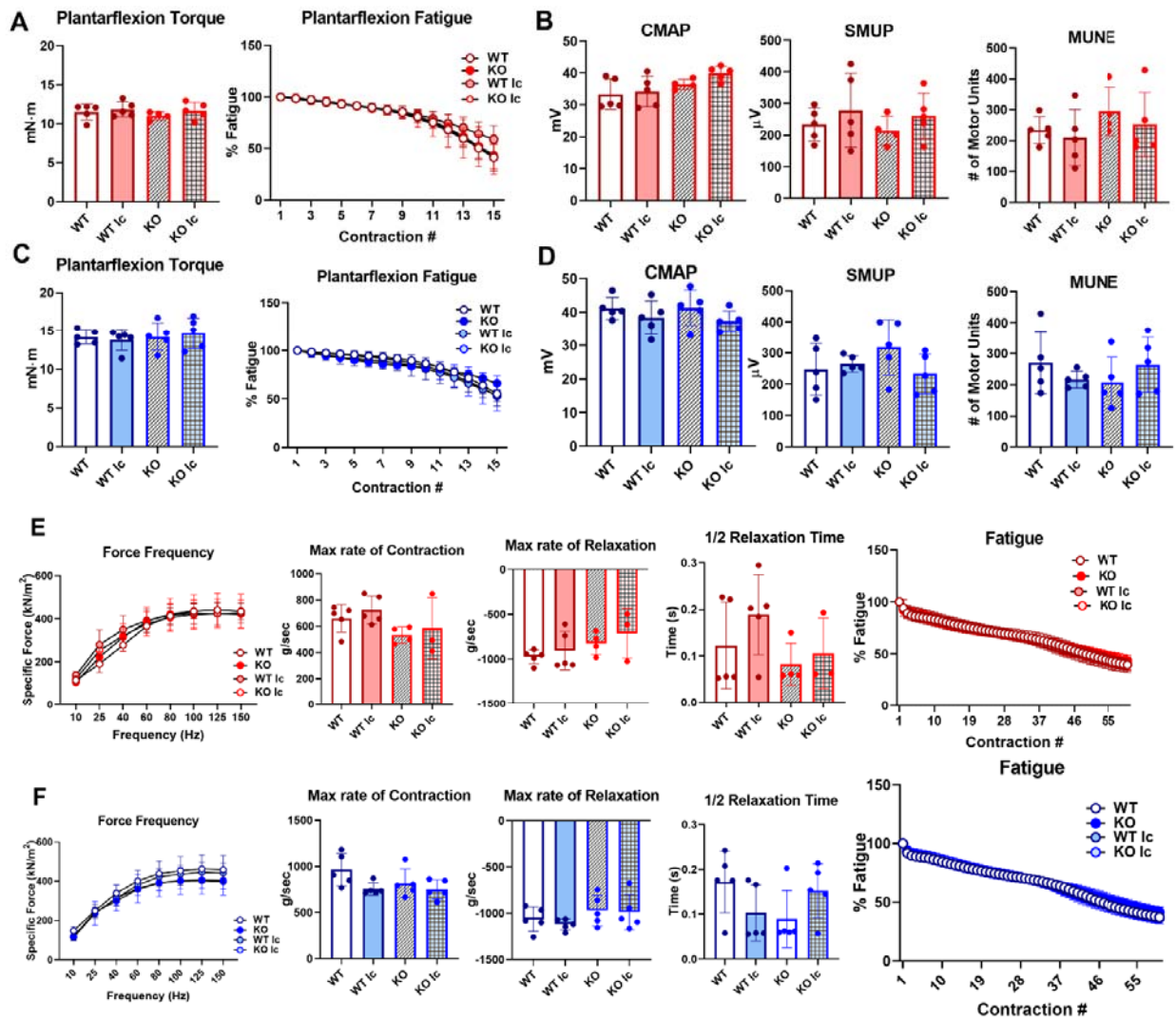
1145 The osteocyte transcriptome data has been deposited into the NCBI GEO
1146 database. The accession number for the data is GSE242445.



1147
1148
1149 **Supplementary Figure 1: Pup numbers for the lactation experiment and**
1150 **body weight measurements for the low-calcium-diet experiment**

1151 Panel A shows total pup numbers in WT and KO female mice that underwent
1152 pregnancy and 2 weeks of lactation. There is no significant differences in the pup
1153 numbers between genotypes. Students t-test was performed for statistical analysis. n=
1154 8/group.

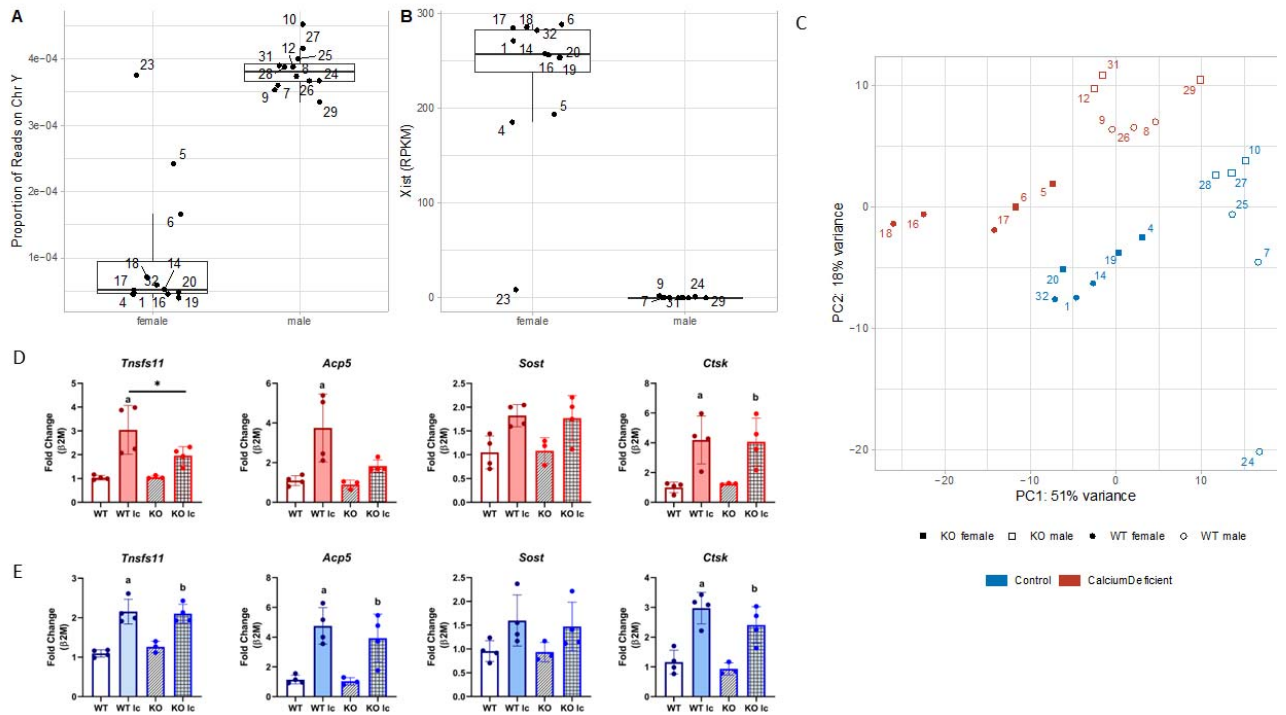
1155 Panels B and C show total body weight of WT and KO female (B) and male (C)
1156 mice. No statistically significant difference was found among the groups, regardless of
1157 genotype or diet. 2-way ANOVA was performed. n= 4-5/group. As depicted here, red is
1158 female, and blue is male.



1159
1160 **Supplementary Figure 2: Neither genotype nor dietary calcium alters**
1161 **muscle functions *in vivo* or *ex vivo***

1162 Panels A and C show *in vivo* muscle plantarflexion force (reported as
1163 plantarflexion torque and plantarflexion fatigue) in WT and KO female (A) and male (C)
1164 mice on a control or a low calcium diet, panels B and D show muscle electrophysiology
1165 parameters of CMAP, SMUP, and MUNE in WT and KO female (B) and male (D) mice,
1166 and panels E and F show *ex vivo* EDL functional measurement (reported as specific
1167 force frequency, maximum rate of contraction, maximum rate of relaxation, half-
1168 relaxation time, and % fatigue) in WT and KO female (E) and male (F) mice

1169 2-way ANOVA was performed. n= 4-5/group. As depicted here, red is female,
1170 and blue is male.



Supplementary Figure 3: Quality control and validation of RNA sequencing

Sanity check of data on the sample's sex. A: Boxplot of proportional of reads on chromosome Y. Male should have a higher value than female. B: Boxplot of RPKM of *Xist*. Males should have very low expression of *Xist*.

C: Scatter plot of PC1 and PC2 from Principal Component Analysis (PCA) of gene expression data.

D: qPCR analysis of *Tnsfs11*, *Acp5*, *Sost*, and *Ctsk* genes from osteocyte-enriched bone chips from female samples. n= 3-4/sample. Two-way ANOVA was performed for statistical analysis. Gene fold-change was normalized using β -2-microglobulin as the housekeeping gene. a= Significantly different from WT, b= Significantly different from KO, *= p < 0.05.

E: qPCR analysis of *Tnsfs11*, *Acp5*, *Sost*, and *Ctsk* genes from osteocyte-enriched bone chips from male samples. n= 3-4/sample. Two-way ANOVA was performed for statistical analysis. Gene fold-change was normalized using β -2-microglobulin as the housekeeping gene. a= Significantly different from WT, b= Significantly different from KO, *= p < 0.05.

Bone Parameters	Virgin		Lactation	
	WT	KO	WT	KO
Femoral cortical bone parameters				
Ct. B. Ar/T. Ar (%)	47.4 ± 1.2	48 ± 1	35.2 ± 1.8 ^a	37.5 ± 1.8 ^{b, c}
Ct. Th (mm)	0.18 ± 0.004	0.19 ± 0.005	0.13 ± 0.004 ^a	0.14 ± 0.01 ^{b, c}
Ps. Pm (mm)	5.16 ± 0.2	5.2 ± 0.06	5.18 ± 0.16	5.2 ± 0.14
Es. Pm (mm)	3.95 ± 0.1	4 ± 0.13	4.4 ± 0.11 ^a	4.3 ± 0.09 ^b
Marrow cavity area (mm ²)	0.93 ± 0.1	0.93 ± 0.04	1.16 ± 0.05 ^a	1.13 ± 0.05 ^b
Femoral trabecular bone parameters				
BV/TV (%)	3.7 ± 1	4.5 ± 0.8	3.1 ± 0.7	4 ± 1.1
Tb. Th (mm)	0.043 ± 0.002	0.044 ± 0.001	0.039 ± 0.002 ^a	0.039 ± 0.001 ^b
Tb. Sp (mm)	0.37 ± 0.05	0.36 ± 0.03	0.57 ± 0.15 ^a	0.44 ± 0.09
Tb. N (1/mm)	0.85 ± 0.2	1.06 ± 0.2	0.8 ± 0.2	1.04 ± 0.25

1188

Bone parameters	Change	% Change	
		WT	KO
Cortical Bone Area Fraction	Decrease	26%	22% *
Cortical Thickness	Decrease	29%	24% *
Ultimate Force	Decrease	38%	31% *
Osteoclast Number/ bone parameter	Increase	141%	129%
TRAP-positive osteocytes	Increase	101%	175% *
Lacunar Area	Increase	26%	15% *
Serum RANKL	Increase	170%	80% *

1189

Supplementary Table 1: FNDC5 KO mice femurs are partially resistant to lactation-induced bone loss.

1190

1191

Femoral cortical and trabecular bone parameters of WT and FNDC5 KO female virgin and lactation mice. n = 5-8/group. Data presented as mean ± standard deviation.

1192

1193

a= significant compared to WT control, b= significant compared to KO control, c= significant compared to WT low Ca diet, 2-way ANOVA, significance <0.05, n= 8/group.

1194

1195
1196
1197

Percentage change in different bone and serum parameters in WT and FNDC5 KO female mice with lactation. *= p<0.05 compared to WT.

Bone Parameters	Female Normal Diet		Female Low Ca Diet		Male Normal Diet		Male Low Ca Diet	
	WT	KO	WT	KO	WT	KO	WT	KO
Ex vivo femur DXA								
BMD (mg/cm ²)	75.4± 2.4	76.6± 1.5	65.4± 4.3 ^a	71.4± 3.4 ^c	74.6± 1.5	78.3± 3 ^a	68.2± 3	68.1± 2 ^b
BMC (g)	0.03± 0.002	0.03± 0.001	0.024± 0.002 ^a	0.027± 0.002 ^{b,c}	0.029± 0.002	0.032± 0.004	0.026± 0.002	0.025± 0.003 ^b
Femoral cortical bone parameters								
Ct.	47.8±	48.4±	41.6±	45.2±	40.1±	43.6±	38.3±	39.1±
B.Ar/T.Ar%	1.6	0.4	1.1 ^a	1.4 ^{b,c}	1.4	0.6 ^a	0.9	1.2 ^b
Ct. Th (mm)	0.2± 0.01	0.2± 0.01	0.15± 0.01 ^a	0.17± 0.01 ^{b,c}	0.15± 0.01	0.2± 0.01 ^a	0.14± 0.01	0.14± 0.01 ^b
Marrow Cavity Area	0.92 ± 0.04	0.86± 0.02	1.02 ± 0.06 ^a	0.9 ± 0.02 ^c	1.1 ± 0.04	1.03 ± 0.06 ^a	1.2 ± 0.03	1.08 ± 0.03 ^c
Femoral trabecular bone parameters								
BV/TV (%)	3.6 ± 1.2	4.3 ± 1	3.2 ± 1	3.9 ± 1	6.1 ± 1.1	8.7 ± 1.9	5.3 ± 1.2	6.4 ±0.6
Tb. Th (mm)	0.059± 0.002	0.059± 0.004	0.056± 0.002	0.055± 0.001	0.036 ±0.001	0.035 ± 0.001	0.035±0. 001	0.035 ± 0.002
Tb. Sp (mm)	0.38 ± 0.03	0.35 ± 0.02	0.51 ± 0.12 ^a	0.48 ± 0.08 ^b	0.274± 0.025	0.235 ± 0.021	0.278 ± 0.027	0.265 ± 0.01
Tb. N (1/mm)	0.81 ± 0.2	0.95 ± 0.14	0.7 ± 0.02	0.91 ±0.13	1.7 ± 0.34	2.5 ^a ± 0.5	1.5 ± 0.3	1.8 ± 0.1
Femoral mechanical properties								
Ultimate Force (N)	19±1	19.4± 1.15	14.8± 0.7 ^a	16.4± 0.5 ^b	18.3± 1	17.6± 0.9	15± 1.3 ^a	12.7± 1.5 ^{b,c}
Stiffness (N/mm)	78.6± 3.2	79.1± 4.9	56.8± 5 ^a	67± 4.3	76.7± 5.6	56.4± 4.75 ^a	56± 10.2 ^a	48.5± 4.9 ^{b,c}
Energy to Failure (N)	2.9± 0.3	3.1± 0.6	1.8± 0.5 ^a	2± 0.3 ^b	3.6± 0.9	3.01± 0.6	2.5± 0.3 ^a	2.35± 0.14

1198
1199

Supplementary Table 2: WT and FNDC5 KO female and male mice bone responds differently to a low-calcium diet

1200 Femoral BMD, BMC, cortical and trabecular bone parameters, and mechanical
1201 properties of 4-5-month-old WT and KO female and male mice under a normal diet or a 2-week
1202 low calcium diet. n = 5/group. Data presented as mean \pm standard deviation.

1203 a= significant compared to WT control, b= significant compared to KO control, c=
1204 significant compared to WT low Ca diet, 2-way ANOVA, significance <0.05 , n= 4-5/group.

1205

References

1206

1207

1208

1209

1210

1211

1212

1213

1214

1215

1216

1217

1218

1219

1220

1221

1222

1223

1224

1225

1226

1227

1228

1229

1230

1231

1232

1233

1234

1235

1236

1237

Andersson G, Ek-Rylander B, Hollberg K, Ljusberg-Sjölander J, Lång P, Norgård M, Wang Y, Zhang SJ. TRACP as an osteopontin phosphatase. *J Bone Miner Res*. 2003; 18(10):1912–1917.

Ardeshirpour L, Dumitru C, Dann P, Sterpka J, VanHouten J, Kim W, Kostenuik P, Wysolmerski J. OPG Treatment Prevents Bone Loss During Lactation But Does Not Affect Milk Production or Maternal Calcium Metabolism. *Endocrinology*. 2015; 156(8):2762–73.

Bao JF, She QY, Hu PP, Jia N, Li A. Irisin, a fascinating field in our times. *Trends Endocrinol Metab*. 2022; 33(9):601–613.

Bélanger LF. Osteocytic osteolysis. *Calcif Tissue Res*. 1969; 4(1):1–12.

Body JJ, Terpos E, Tombal B, Hadji P, Arif A, Young A, Aapro M, Coleman R. Bone health in the elderly cancer patient: A SIOG position paper. *Cancer Treat Rev*. 2016; 51:46–53.

Bonewald L. Use it or lose it to age: A review of bone and muscle communication. *Bone*. 2019; 120:212–218.

Bonewald LF. The amazing osteocyte. *J Bone Miner Res*. 2011; 26(2):229–267.

Bostrom P, Wu J, Jedrychowski MP, Korde A, Ye L, Lo JC, Rasbach KA, Boström EA, Choi JH, Long JZ, Kajimura S, Zingaretti MC, Vind BF, Tu H, Cinti S, Højlund K, Gygi SP, Spiegelman BM. A PGC1-alpha-dependent myokine that drives brown-fat-like development of white fat and thermogenesis. *Nature*. 2012; 481(7382):463–471.

Bouxsein ML, Boyd SK, Christiansen BA, Guldberg RE, Jepsen KJ, Müller R. Guidelines for assessment of bone microstructure in rodents using micro-computed tomography. *J Bone Miner Res*. 2010; 25(7):1468–86.

Breese MR, Liu Y. NGSUtils: a software suite for analyzing and manipulating next-generation sequencing datasets. *Bioinformatics*. 2013; 29(4):494–500.

Brotto M, Bonewald L. Bone and muscle: Interactions beyond mechanical. *Bone*. 2015; 80:109–114.

Buenzli PR, Sims NA. Quantifying the osteocyte network in the human skeleton. *Bone*. 2015; 75:144–150.

Celi FS, Brown H. Adipose Tissue Plasticity: Hormonal and Environmental Manipulation, in *Hormones*. Spiegelman B, editor, Springer Copyright; 2017.

Colaiani G, Cuscito C, Mongelli T, Oranger A, Mori G, Brunetti G, Colucci S, Cinti S, Grano M. Irisin enhances osteoblast differentiation in vitro. *Int J Endocrinol*. 2014; p. 902186–902186.

Colaiani G, Cuscito C, Mongelli T, Pignataro P, Buccoliero C, Liu P, Lu P, Sartini L, Di Comite M,

- 1238 Mori G, Di Benedetto A, Brunetti G, Yuen T, Sun L, Reseland JE, Colucci S, New MI, Zaidi M, Cinti
1239 S, Grano M. The myokine irisin increases cortical bone mass. *Proc Natl Acad Sci.* 2015;
1240 112(39):12157–62.
- 1241 **Colaiani G**, Mongelli T, Cuscito C, Pignataro P, Lippo L, Spiro G, Notarnicola A, Severi I, Passeri G,
1242 Mori G, Brunetti G, Moretti B, Tarantino U, Colucci SC, Reseland JE, Vettor R, Cinti S, Grano M. Irisin
1243 prevents and restores bone loss and muscle atrophy in hind-limb suspended mice. *Sci Rep*, 2017; 7(1): p.
1244 2811.
- 1245 **Colaiani G**, Grano M. Role of Irisin on the bone-muscle functional unit. *Bonekey Rep*, 2015; 4: p. 765.
- 1246 **Colucci SC**, Buccoliero C, Sanesi L, Errede M, Colaiani G, Annese T, Khan MP, Zerlotin R, Dicarolo
1247 M, Schipani E, Kozloff KM, Grano M. Systemic Administration of Recombinant Irisin Accelerates
1248 Fracture Healing in Mice. *Int J Mol Sci.* 2019; p. 22–22.
- 1249 **Dallas SL**, Prideaux M, Bonewald LF. The osteocyte: an endocrine cell ... and more. *Endocr Rev.*
1250 2013; 34(5):658–90.
- 1251 **Dobin A**, Davis CA, Schlesinger F, Drenkow J, Zaleski C, Jha S, Batut P, Chaisson M, Gingeras
1252 TR. STAR: ultrafast universal RNA-seq aligner. *Bioinformatics.* 2013; 29(1):15–21.
- 1253 **Dole NS**, Yee CS, Mazur CM, Acevedo C, Alliston T. TGF β Regulation of
1254 Perilacunar/Canalicular Remodeling Is Sexually Dimorphic. *J Bone Miner Res.* 2020; 35(8):1549-
1255 1561.
- 1256 **During A**. Osteoporosis: A role for lipids. *Biochimie.* 2020; 178:49–55.
- 1257 **Erickson HP**. Irisin and FNDC5 in retrospect: An exercise hormone or a transmembrane receptor? *Adipocyte*,
1258 2013; 2(4): p. 289-93.
- 1259 **Essex AL**, Huot JR, Deosthale P, Wagner A, Figueras J, Davis A, Damrath J, Pin F, Wallace J, Bonetto
1260 A, Plotkin LI. Triggering Receptor Expressed on Myeloid Cells 2 (TREM2) R47H Variant Causes Distinct
1261 Age- and Sex-Dependent Musculoskeletal Alterations in Mice. *J Bone Miner Res.* 2022; 37(7):1366–1381.
- 1262 **Estell EG**, Le PT, Vegting Y, Kim H, Wrann C, Bouxsein ML, Nagano K, Baron R, Spiegelman BM,
1263 Rosen CJ. Irisin directly stimulates osteoclastogenesis and bone resorption in vitro and in vivo. *Elife.*
1264 2020; p. 2020–2029.
- 1265 **Farley JR**, Baylink DJ. Skeletal alkaline phosphatase activity as a bone formation index in vitro.
1266 *Metabolism.* 1986; 35(6):563–71.
- 1267 **Feng JQ**, Ye L, Schiavi S. Do osteocytes contribute to phosphate homeostasis? *Curr Opin Nephrol*
1268 *Hypertens.* 2009; 18(4):285–91.
- 1269 **Geng W**, Wright GL. Skeletal sensitivity to dietary calcium deficiency is increased in the female
1270 compared with the male rat. *Can J Physiol Pharmacol.* 2001; 79(5):379–85.
- 1271 **The Gene Ontology Resource: enriching a GOLD mine TGO.** *Nucleic Acids Res.* 2021;

- 1272 49(D1):325–334.
- 1273 **Goltzman D.** Studies on the mechanisms of the skeletal anabolic action of endogenous and
1274 exogenous parathyroid hormone. *Arch Biochem Biophys.* 2008; 473(2):218–242.
- 1275 **Gu Z.** Complex heatmap visualization. *iMeta*, 2022; 1(3): p. e43.
- 1276 **Hamrick MW, Samaddar T, Pennington C, McCormick J.** Increased muscle mass with myostatin
1277 deficiency improves gains in bone strength with exercise. *J Bone Miner Res.* 2006; 21(3):477–83.
- 1278 **Huot JR, Pin F, Essex AL, Bonetto A.** MC38 Tumors Induce Musculoskeletal Defects in Colorectal
1279 Cancer. *Int J Mol Sci.* 2021; 22(3).
- 1280 **Huot JR, Pin F, Chatterjee R, Bonetto A.** PGC1 α overexpression preserves muscle mass and
1281 function in cisplatin-induced cachexia. *J Cachexia Sarcopenia Muscle.* 2022; 13(5):2480–2491.
- 1282 **Islam MR, Valaris S, Young MF, Haley EB, Luo R, Bond SF, Mazuera S, Kitchen RR, Caldarone BJ,**
1283 **Bettio LEB, Christie BR, Schmider AB, Soberman RJ, Besnard A, Jedrychowski MP, Kim H, Tu H,**
1284 **Kim E, Choi SH, Tanzi RE, Spiegelman BM, Wrann CD.** Exercise hormone irisin is a critical regulator
1285 of cognitive function. *Nat Metab.* 2021; (8):1058–1070.
- 1286 **Jahn K, Kelkar S, Zhao H, Xie Y, Tiede-Lewis LM, Dusevich V, Dallas SL, Bonewald LF.** Osteocytes
1287 Acidify Their Microenvironment in Response to PTHrP In Vitro and in Lactating Mice In Vivo. *J Bone*
1288 *Miner Res.* 2017; 32(8):1761–1772.
- 1289 **Jähn-Rickert K, Zimmermann EA.** Potential Role of Perilacunar Remodeling in the Progression of
1290 Osteoporosis and Implications on Age-Related Decline in Fracture Resistance of Bone. *Curr*
1291 *Osteoporos Rep.* 2021; 19(4):391–402.
- 1292 **Jo D, Song J.** Irisin Acts via the PGC-1 α and BDNF Pathway to Improve Depression-like Behavior.
1293 *Clin Nutr Res.* 2021; 10(4):292–302.
- 1294 **Johannesdottir F, Aspelund T, Reeve J, Poole KE, Sigurdsson S, Harris TB, Gudnason VG,**
1295 **Sigurdsson G.** Similarities and differences between sexes in regional loss of cortical and trabecular
1296 bone in the mid-femoral neck: the AGES-Reykjavik longitudinal study. *J Bone Miner Res.* 2013;
1297 28(10):2165–76.
- 1298 **Johnston CB, Dagar M.** Osteoporosis in Older Adults. *Med Clin North Am.* 2020; 104(5):873–884.
- 1299 **Kalkwarf HJ.** Lactation and maternal bone health. *Adv Exp Med Biol.* 2004; 554:101–115.
- 1300 **Kaplan MM.** Alkaline phosphatase. *N Engl J Med.* 1972; 286(4):200–202.
- 1301 **Karsenty G, Mera P.** Molecular bases of the crosstalk between bone and muscle. *Bone.* 2018;
1302 115:43–49.
- 1303 **Kawao N, Moritake A, Tatsumi K, Kaji H.** Roles of Irisin in the Linkage from Muscle to Bone During
1304 Mechanical Unloading in Mice. *Calcif Tissue Int.* 2018; 103(1):24–34.

- 1305 **Kim H**, Wrann CD, Jedrychowski M, Vidoni S, Kitase Y, Nagano K, Zhou C, Chou J, Parkman VA,
1306 Novick SJ, Strutzenberg TS, Pascal BD, Le PT, Brooks DJ, Roche AM, Gerber KK, Mattheis L, Chen
1307 W, Tu H, Bouxsein ML, Griffin PR, Baron R, Rosen CJ, Bonewald LF, Spiegelman BM. Irisin
1308 Mediates Effects on Bone and Fat via α V Integrin Receptors. *Cell*. 2018; 175(7):17–17.
- 1309 **Kitase Y**, Vallejo JA, Gutheil W, Vemula H, Jähn K, Yi J, Zhou J, Brotto M, Bonewald LF. β -
1310 aminoisobutyric Acid, I-BAIBA, Is a Muscle-Derived Osteocyte Survival Factor. *Cell Rep*. 2018;
1311 22(6):1531–1544.
- 1312 **Korta P**, Pocheć E, Mazur-Biały A. Irisin as a Multifunctional Protein: Implications for Health and
1313 Certain Diseases. *Medicina (Kaunas)*, 2019; 55(8).
- 1314 **Kovacs CS**. Calcium and bone metabolism in pregnancy and lactation. *The Journal of clinical*
1315 *endocrinology and metabolism*. 2001; (6):86–86.
- 1316 **Kumssa DB**, Joy EJ, Ander EL, Watts MJ, Young SD, Walker S, Broadley MR. Dietary calcium and zinc
1317 deficiency risks are decreasing but remain prevalent. *Sci Rep*, 2015; 5: p. 10974.
- 1318 **Kurapaty SS**, Hsu WK. Sex-Based Difference in Bone Healing: A Review of Recent Preclinical
1319 Literature. *Curr Rev Musculoskelet Med*. 2022.
- 1320 **Lee HJ**, Lee JO, Kim N, Kim JK, Kim HI, Lee YW, Kim SJ, Choi JI, Oh Y, Kim JH, Suyeon-Hwang,
1321 Park SH, Kim HS. Irisin, a Novel Myokine, Regulates Glucose Uptake in Skeletal Muscle Cells via
1322 AMPK. *Mol Endocrinol*. 2015; 29(6):873–81.
- 1323 **Liao Y**, Smyth GK, Shi W. featureCounts: an efficient general purpose program for assigning
1324 sequence reads to genomic features. *Bioinformatics*. 2014; 30(7):923–953.
- 1325 **Liu Q**, Lei L, Yu T, Jiang T, Kang Y. Effect of Brain-Derived Neurotrophic Factor on the
1326 Neurogenesis and Osteogenesis in Bone Engineering. *Tissue Eng Part A*. 2018; 24:1283–1292.
- 1327 **Love MI**, Huber W, Anders S. Moderated estimation of fold change and dispersion for RNA-seq data
1328 with DESeq2. *Genome Biol*. 2014; 15(12):550–550.
- 1329 **Lu D**, Demissie S, Horowitz NB, Gower AC, Lenburg ME, Alekseyev YO, Hussein AI, Bragdon B, Liu Y,
1330 Daukss D, Page JM, Webster MZ, Schlezinger JJ, Morgan EF, Gerstenfeld LC. Temporal and
1331 Quantitative Transcriptomic Differences Define Sexual Dimorphism in Murine Postnatal Bone Aging.
1332 *JBMR Plus*, 2022; 6(2): p. e10579.
- 1333 **Luo X**, Li J, Zhang H, Wang Y, Shi H, Ge Y, Yu X, Wang H, Dong Y. Irisin promotes the browning of
1334 white adipocytes tissue by AMPK α 1 signaling pathway. *Res Vet Sci*. 2022; 152:270–276.
- 1335 **Ma Y**, Qiao X, Zeng R, Cheng R, Zhang J, Luo Y, Nie Y, Hu Y, Yang Z, Zhang J, Liu L, Xu W, Xu
1336 CC, Xu L. Irisin promotes proliferation but inhibits differentiation in osteoclast precursor cells. *Faseb j*.
1337 2018; p. 201700983–201700983.
- 1338 **Maak S**, Norheim F, Drevon CA, Erickson HP. Progress and Challenges in the Biology of FNDC5

- 1339 and Irisin. *Endocr Rev.* 2021; 42(4):436–456.
- 1340 **Matikainen N**, Pekkarinen T, Ryhänen EM, Schalin-Jäntti C. Physiology of Calcium Homeostasis: An
1341 Overview. *Endocrinol Metab Clin North Am.* 2021; 50(4):575–590.
- 1342 **Melville KM**, Robling AG, Meulen MCVD. In vivo axial loading of the mouse tibia. *Methods Mol Biol.*
1343 2015; 1226:99–115.
- 1344 **Mo C**, Zhao R, Vallejo J, Igwe O, Bonewald L, Wetmore L, Brotto M. Prostaglandin E2 promotes
1345 proliferation of skeletal muscle myoblasts via EP4 receptor activation. *Cell Cycle.* 2015; 14(10):1507–
1346 1523.
- 1347 **Moreno-Layseca P**, Icha J, Hamidi H, Ivaska J. Integrin trafficking in cells and tissues. *Nat Cell Biol.*
1348 2019; 21(2):122– 132.
- 1349 **Mu A**, Wales TE, Zhou H, Draga-Coletă SV, Gorgulla C, Blackmore KA, Mittenbühler MJ, Kim CR,
1350 Bogoslavski D, Zhang Q, Wang ZF, Jedrychowski MP, Seo HS, Song K, Xu AZ, Sebastian L, Gygi
1351 SP, Arthanari H, Dhe-Paganon S, Griffin PR, Engen JR, Spiegelman BM. Irisin acts through its
1352 integrin receptor in a two-step process involving extracellular Hsp90 α . *Mol Cell.* 2023; 83(11):1903–
1353 1920.
- 1354 **Muruganandan S**, Sinal CJ. The impact of bone marrow adipocytes on osteoblast and
1355 osteoclast differentiation. *IUBMB Life.* 2014; 66(3):147–155.
- 1356 **Nakashima T**, Hayashi M, Fukunaga T, Kurata K, Oh-Hora M, Feng JQ, Bonewald LF, Kodama
1357 T, Wutz A, Wagner EF, Penninger JM, Takayanagi H. Evidence for osteocyte regulation of bone
1358 homeostasis through RANKL expression. *Nat Med.* 2011; 17(10):1231–1235.
- 1359 **Ono T**, Hayashi M, Sasaki F, Nakashima T. RANKL biology: bone metabolism, the immune system, and
1360 beyond. *Inflamm Regen*, 2020; 40: p. 2.
- 1361 **Osipov B**, Paralkar MP, Emami AJ, Cunningham HC, Tjandra PM, Pathak S, Langer HT, Baar K,
1362 Christiansen BA. Sex differences in systemic bone and muscle loss following femur fracture in mice.
1363 *J Orthop Res.* 2022; (4):878–890.
- 1364 **Perakakis N**, Triantafyllou GA, Fernández-Real JM, Huh JY, Park KH, Seufert J, Mantzoros CS.
1365 Physiology and role of irisin in glucose homeostasis. *Nat Rev Endocrinol.* 2017; 13(6):324–337.
- 1366 **Pin F**, Prideaux M, Huot JR, Essex AL, Plotkin LI, Bonetto A, Bonewald LF. Non-bone metastatic
1367 cancers promote osteocyte-induced bone destruction. *Cancer Lett.* 2021; 520:80–90.
- 1368 **Pin F**, Jones AJ, Huot JR, Narasimhan A, Zimmers TA, Bonewald LF, Bonetto A. RANKL
1369 Blockade Reduces Cachexia and Bone Loss Induced by Non-Metastatic Ovarian Cancer in
1370 Mice. *J Bone Miner Res.* 2022; 37(3):381–396.
- 1371 **Posa F**, Colaianni G, Di Cosola M, Dicarolo M, Gaccione F, Colucci S, Grano M, Mori G. The
1372 Myokine Irisin Promotes Osteogenic Differentiation of Dental Bud-Derived MSCs. *Biology.* 2021;

- 1373 (4).
- 1374 **Qi JY**, Yang LK, Wang XS, Wang M, Li XB, Feng B, Wu YM, Zhang K, Liu SB. Irisin: A promising
1375 treatment for neurodegenerative diseases. *Neuroscience*. 2022; 498:289–299.
- 1376 **Qing H**, Ardeshirpour L, Pajevic PD, Dusevich V, Jähn K, Kato S, Wysolmerski J, Bonewald LF.
1377 Demonstration of osteocytic perilacunar/canalicular remodeling in mice during lactation. *J Bone*
1378 *Miner Res*. 2012; 27(5):1018–1047.
- 1379 **Qing H**, Bonewald LF. Osteocyte remodeling of the perilacunar and pericanalicular matrix.
1380 *International Journal of Oral Science*. 2009.
- 1381 **Robling AG**, Bonewald LF. The Osteocyte: New Insights. *Annu Rev Physiol*. 2020; 82:485– 506.
- 1382 **Rosen CJ**, Bouxsein ML. Mechanisms of disease: is osteoporosis the obesity of bone? *Nat Clin*
1383 *Pract Rheumatol*. 2006; 2(1):35–43.
- 1384 **Saedi A**, Bermeo S, Plotkin L, Myers DE, Duque G. Mechanisms of palmitate-induced
1385 lipotoxicity in osteocytes. *Bone*. 2019; 127:353–359.
- 1386 **Saedi A**, Chen L, Phu S, Vogrin S, Miao D, Ferland G, Gaudreau P, Duque G. Age-Related
1387 Increases in Marrow Fat Volumes have Regional Impacts on Bone Cell Numbers and Structure.
1388 *Calcif Tissue Int*. 2020; 107(2):126–134.
- 1389 **Schwartz AV**. Marrow fat and bone: review of clinical findings. *Front Endocrinol (Lausanne)*, 2015; 6: p.
1390 40.
- 1391 **Sharma A**, Michels LV, Pitsillides AA, Greeves J, Plotkin LI, Cardo V, Sims NA, Clarkin CE. Sexing
1392 Bones: Improving Transparency of Sex Reporting to Address Bias Within Preclinical Studies. *J Bone*
1393 *Miner Res*. 2023; 38(1):5–13.
- 1394 **Shimonty A**, Bonewald LF, Pin F. Role of the Osteocyte in Musculoskeletal Disease. *Curr*
1395 *Osteoporos Rep*. 2023; 21(3):303–310.
- 1396 **Silver IA**, Murrills RJ, Etherington DJ. Microelectrode studies on the acid microenvironment beneath
1397 adherent macrophages and osteoclasts. *Exp Cell Res*. 1988; 175(2):266–76.
- 1398 **Styner M**, Pagnotti GM, Galior K, Wu X, Thompson WR, Uzer G, Sen B, Xie Z, Horowitz MC,
1399 Styner MA, Rubin C, Rubin J. Exercise Regulation of Marrow Fat in the Setting of PPAR μ Agonist
1400 Treatment in Female C57BL/6 Mice. *Endocrinology*. 2015; 156(8):2753–61.
- 1401 **Team RC**. R: A Language and Environment for Statistical Computing. 2022, R Foundation for
1402 Statistical Computing. In: 2022.
- 1403 **Temiyasathit S**, Jacobs CR. Osteocyte primary cilium and its role in bone mechanotransduction.
1404 *Ann N Y Acad Sci*. 2010; 1192:422–430.
- 1405 **Teti A**, Zallone A. Do osteocytes contribute to bone mineral homeostasis? Osteocytic osteolysis
1406 revisited. *Bone*. 2009; 44(1):11–17.

- 1407 **Tsourdi E**, Jähn K, Rauner M, Busse B, Bonewald LF. Physiological and pathological osteocytic
1408 osteolysis. *J Musculoskelet Neuronal Interact.* 2018; 18(3):292–303.
- 1409 **Tsourdi E**, Anastasilakis AD, Hofbauer LC, Rauner M, Lademann F. Irisin and Bone in Sickness and
1410 in Health: A Narrative Review of the Literature. *J Clin Med.* 2022; (22):11–11.
- 1411 **Uda Y**, Azab E, Sun N, Shi C, Pajevic PD. Osteocyte Mechanobiology. *Curr Osteoporos Rep*, 2017;
1412 15(4): p. 318-325.
- 1413 **Wang H**, Zhao YT, Zhang S, Dubielecka PM, Du J, Yano N, Chin YE, Zhuang S, Qin G, Zhao TC.
1414 Irisin plays a pivotal role to protect the heart against ischemia and reperfusion injury. *J Cell Physiol.*
1415 2017; 232(12):3775–3785.
- 1416 **Wickham H**. GGPlot2: Elegant Graphics for Data Analysis. New York: Springer-Verlag; 2016.
- 1417 **Wrann CD**, White JP, Salogiannis J, Laznik-Bogoslavski D, Wu J, Ma D, Lin JD, Greenberg ME,
1418 Spiegelman BM. Exercise induces hippocampal BDNF through a PGC-1 α /FNDC5 pathway. *Cell*
1419 *Metab.* 2013; 18(5):649–59.
- 1420 **Wu T**. clusterProfiler 4.0: A universal enrichment tool for interpreting omics data. *Innovation (Camb)*,
1421 2021; 2(3): p. 100141.
- 1422 **Wysolmerski JJ**. The evolutionary origins of maternal calcium and bone metabolism during lactation.
1423 *J Mammary Gland Biol Neoplasia.* 2002; 7(3):267–76.
- 1424 **Wysolmerski JJ**. Osteocytic osteolysis: time for a second look? *Bonekey Rep*, 2012; 1: p. 229.
- 1425 **Wysolmerski JJ**. Osteocytes remove and replace perilacunar mineral during reproductive cycles. *Bone.*
1426 2013; 54(2):230–236.
- 1427 **Xin C**, Liu J, Zhang J, Zhu D, Wang H, Xiong L, Lee Y, Ye J, Lian K, Xu C, Zhang L, Wang Q, Liu Y,
1428 Tao L. Irisin improves fatty acid oxidation and glucose utilization in type 2 diabetes by regulating the
1429 AMPK signaling pathway. *Int J Obes.* 2016; 40(3):443–51.
- 1430 **Xiong J**, Piemontese M, Onal M, Campbell J, Goellner JJ, Dusevich V, Bonewald L, Manolagas SC,
1431 O'Brien CA. Osteocytes, not Osteoblasts or Lining Cells, are the Main Source of the RANKL
1432 Required for Osteoclast Formation in Remodeling Bone. *PLoS One.* 2015; 10(9):138189– 138189.
- 1433 **Xiong J**, O'Brien CA. Osteocyte RANKL: new insights into the control of bone remodeling. *J Bone*
1434 *Miner Res.* 2012; 27(3):499–505.
- 1435 **Yeung DK**, Griffith JF, Antonio GE, Lee FK, Woo J, Leung PC. Osteoporosis is associated with
1436 increased marrow fat content and decreased marrow fat unsaturation: a proton MR spectroscopy
1437 study. *J Magn Reson Imaging.* 2005; 22(2):279–85.
- 1438 **Youlten SE**, Kemp JP, Logan JG, Ghirardello EJ, Sergio CM, Dack MRG, Guilfoyle SE, Leitch
1439 VD, Butterfield NC, Komla-Ebri D, Chai RC, Corr AP, Smith JT, Mohanty ST, Morris JA,
1440 McDonald MM, Quinn JMW, McGlade AR, Bartonicek N, Jansson M, Hatzikotoulas K, Irving MD,
1441 Beleza-Meireles A, Rivadeneira F, Duncan E, Richards JB, Adams DJ, Lelliott CJ, Brink R, Phan

1442 TG, Eisman JA, Evans DM, Zeggini E, Baldock PA, Bassett JHD, Williams GR, Croucher PI.
1443 Osteocyte transcriptome mapping identifies a molecular landscape control- ling skeletal
1444 homeostasis and susceptibility to skeletal disease. *Nat Commun.* 2021; 12(1):2444–2444.

1445 **Young MF**, Valaris S, Wrann CD. A role for FNDC5/Irisin in the beneficial effects of exercise on the
1446 brain and in neurodegenerative diseases. *Prog Cardiovasc Dis.* 2019; 62(2):172– 178.

1447 **Zhang D**, Bae C, Lee J, Lee J, Jin Z, Kang M, Cho YS, Kim JH, Lee W, Lim SK. The bone
1448 anabolic effects of irisin are through preferential stimulation of aerobic glycolysis. *Bone.* 2018;
1449 114:150–160.

1450 **Zhang H**, Wu X, Liang J, Kirberger M, Chen N. Irisin, an exercise-induced bioactive peptide
1451 beneficial for health promotion during aging process. *Ageing Res Rev.* 2022; 80:101680–101680.

1452 **Zhang Y**, Li R, Meng Y, Li S, Donelan W, Zhao Y, Qi L, Zhang M, Wang X, Cui T, Yang LJ, Tang
1453 D. Irisin stimulates browning of white adipocytes through mitogen-activated protein kinase p38
1454 MAP kinase and ERK MAP kinase signaling. *Diabetes.* 2014; 63(2):514–539.

1455 **Zhu J**, Li J, Yao T, Li T, Chang B, Yi X. Analysis of the role of irisin receptor signaling in regulating
1456 osteogenic/adipogenic differentiation of bone marrow mesenchymal stem cells. *Biotechnol Genet
1457 Eng Rev.* 2023; p. 1–24.
1458